Supplementary Materials for

An optical nanoreporter of endolysosomal lipid accumulation reveals enduring effects of diet on hepatic macrophages in vivo

Thomas V. Galassi[1,2], Prakrit V. Jena[1], Janki Shah[1], Geyou Ao[3], Elizabeth Molitor[4], Yaron Bram[2], Angela Frankel[2], Jiwoon Park[2], Jose Jessurun[2], Daniel S. Ory[4], Adriana Haimovitz-Friedman[1], Daniel Roxbury[5], Jeetain Mittal[6], Ming Zheng[3], Robert E. Schwartz[2], Daniel A. Heller[1,2*]

[1]Memorial Sloan Kettering Cancer Center, New York, NY 10065

[2]Weill Cornell Medical College, New York, NY 10065

[3]National Institute of Standards and Technology, Gaithersburg, MD 20899

[4]Department of Medicine, Washington University School of Medicine, St. Louis, MO 63110

[5]Department of Chemical Engineering, University of Rhode Island, Kingston, RI 02881

[6]Department of Chemical and Biomolecular Engineering, Lehigh University, Bethlehem, PA 18015

Correspondence to: hellerd@mskcc.org

This PDF file includes:

Table of Contents
Supplementary Materials and Methods
Supplementary Text
Supplementary Figs. 1-38
Supplementary Tables 1-2
Tables of individual mouse level data

Materials and Methods

DNA encapsulation of single-walled carbon nanotubes

EG 150X single-walled carbon nanotubes (SWCNT) were purchased from Chasm Advanced Materials. Aqueous dispersions of SWCNTs in ssDNA were produced via probe tip ultrasonication (Sonics & Materials, Inc.) of raw 2 mg/mL ssDNA with 1 mg/mL raw SWCNT powder in 0.1 M NaCl for 120 minutes at ~8 W. Following sonication, aqueous dispersions were centrifuged (Eppendorf 5430 R) for 90 minutes at 17,000 x g. The top 85% of the resulting supernatant was then collected and used for chirality enrichment.

Isolation of single nanotube chiralities

The (9,4) SWCNT was purified from unsorted samples of ssCTTC$_3$TTC-SWCNT using the aqueous two phase separation method (*22, 47, 48*). ssCTTC$_3$TTC-SWCNT was mixed with a solution containing a final concentration of 7.76% polyethylene glycol (PEG, molecular weight 6 kDa, Alfa Aesar), and 15.0% polyacrylamide (PAM, molecular weight 10 kDa, Sigma Aldrich). The sample was then incubated overnight at room temperature, vortexed, and centrifuged at 10,000 x g for 3 minutes. The top phase was then collected and added to blank "bottom phase," which was produced by centrifuging a 7.76% PEG, 15.0% PAM solution at 10,000 x g for 10 minutes and then removing the bottom phase of solution. The resulting solution was then vortexed and centrifuged, and the top phase, which contained highly enriched ssCTTC$_3$TTC-(9,4) was collected. NaSCN was added to the collected top phase at a final concentration of 0.5 M and the resulting solution was incubated at 4 degrees Celsius overnight to precipitate ssCTTC$_3$TTC-(9,4). The sample was then centrifuged at 17,000 x g for 20 minutes which causes

ssCTTC$_3$TTC-(9,4) to pellet. The resulting supernatant was then removed and the pellet was re-suspended in dH$_2$O and stored with 0.1 mg/mL free ssCTTC$_3$TTC for stability.

NIR hyperspectral microscopy of cells and resected tissue sections

NIR hyperspectral microscopy (*30*) was performed by injecting a continuous wave 730 nm diode laser (output power = 2 W), into a multimode fiber to provide an excitation source for experiments. Homogenous illumination over the field of view was assured by passing the excitation beam through a custom beam shaping module to produce a top hat intensity profile with a maximum of 20% variation on the surface of the sample. The laser was reflected into an Olympus IX-71 inverted microscope (with internal optics modified for near infrared transmission) equipped with a 100X (UAPON100XOTIRF, NA=1.49) oil objective (Olympus via a longpass dichroic mirror with a cut-on wavelength of 880 nm. Spatially resolved near-infrared emission from the sample passed through a volume Bragg grating (VBG) so that it could be spectrally defined. Following its passage through the VBG, a specific wavelength component of emitted polychromatic light was diffracted, while all other wavelengths were transmitted through the grating. The diffracted component then passed through the VBG a second time resulting in a monochromatic beam which was collected by a 256 x 320 pixel InGaAs array (Photon Etc.). This method was used to obtain a continuous stack of images for specified wavelength ranges which resulted in hyperspectral cubes wherein every pixel of a near-infrared image was spectrally resolved (*30*).

Analysis and processing of hyperspectral data

Hyperspectral data was saved as 16 bit arrays (320 x 256 x Y), where the first two coordinates represent the spatial location of a pixel and the last coordinate its position in wavelength space (in this study Y ranged from 26-125). Data was analyzed using MATLAB code written by the authors. In brief, for data taken on purified samples of the (9,4) or (7,6) nanotube, a 26-frame wavelength space that ranged from 1100-1200 nm was used. A peak finding algorithm was used to determine the intensity range for a given pixel i.e. range = (intensity_maximum – intensity_minimum). Data points were designated as peaks if their intensity was range/4 greater than the intensity of adjacent pixels. Pixels that did not meet this threshold (primarily due to low signal above background) were removed from data sets. Remaining pixels were fit with a Lorentzian function.

Photoluminescence plots and fluorescence spectroscopy of nanotubes in solution

Photoluminescent excitation/emission spectra of ssDNA-SWCNTs were acquired using an assembly consisting of a SuperK EXTREME supercontinuum white light laser source (NKT photonics), inverted microscope, and InGaAs near-infrared detector. The excitation source was used with a Varia variable bandpass filter accessory capable of tuning the output from 490-825 nm with a bandwidth of 20 nm. The excitation beam was filtered with a long pass dichroic mirror with a cut on wavelength of 900 nm. Excitation light was shaped and fed into the back of an inverted IX-71 microscope (Olympus) and passed through a 20X near-infrared objective (Olympus LCPlan N 0.45 IR) to illuminate 100 µL aqueous sample of nanotubes at a concentration of 0.2 mg/L (sorted nanotube samples) or 1.0 mg/L (unsorted nanotube samples). Emission light was collected through the 20X objective, passed through a dichroic mirror (875 nm, Semrock), and f/# matched to an Isoplane SCT-320 spectrograph (f/4.6, Princeton

Instruments) with a slit width of 410 μm. Emission light was dispersed with a 86 g/mm grating with a blaze wavelength of 950 nm and collected by a NIRvana 640 x 512 pixel InGaAs array (Princeton Instruments). Following acquisition, spectral corrections for wavelength-dependent excitation power, non-linearity in the InGaAs detector response, and background subtraction were applied to data. For fluorescence spectroscopy measurements at a single excitation wavelength, a continuous wave laser with an output power of 1 W was used as the excitation source. This laser emitted at 730 nm, which is close to the resonant excitation maximum of ssCTTC$_3$TTC-(9,4).

Identification of probes for endolysosomal lipid accumulation

The response of four different purified, DNA-sequence, nanotube chirality combinations to lipids in the endolysosomal lumen was investigated. Tested DNA sequence/nanotube chirality combinations included ssCTC$_3$TC-(7,6), ssT$_3$C$_5$T$_3$-(7,6), ssT$_2$C$_4$T$_2$-(9,4), and ssCTTC$_3$TTC-(9,4). In solution, emission spectra were collected following a 6-hour incubation of each DNA-nanotube complex with 0.5 mg/mL low-density lipoprotein (LDL) at 37 degrees Celsius. To the response in cells, RAW 264.7 macrophages were treated for 24 hours with 3 μg/mL U18666A to cause endolysosomal lipid accumulation and then incubated with the aforementioned DNA-nanotube complexes as described in the section below entitled “Reporter validation in live cells”. Six hours after nanotube addition to media, NIR hyperspectral microscopy was performed on cells to measure the nanotube emission wavelength.

Near-infrared, in vivo spectroscopy

Non-invasive in vivo spectra were taken using a custom-built reflectance probe-based spectroscopy system (*41*). Excitation light was provided by injecting a continuous wave 730 nm diode laser (Frankfurt) into a bifurcated fiber optic reflection probe bundle (Thorlabs). The sample leg of the bundle included one 200 μm, 0.22 NA fiber optic cable for sample excitation located in the center of six 200 μm, 0.22 NA fiber optic cables for collection of the emitted light. Excitation power at the sample was ~590 mW with an ~1 cm circle being illuminated. An exposure time of 5 seconds was used for all in vivo data acquisition. Long pass filters were used to filter emission light below 1050 nm, and emission light was focused through a 410 μm slit into a Czerny-Turner spectrograph with 303 mm focal length (Shamrock 303i, Andor). Emission light was dispersed by an 85 g/mm grating with 1350 blaze wavelength and collected by an iDus InGaAs camera (Andor). Following acquisition data was processed to apply spectral corrections for non-linearity of the InGaAs detector response, background subtraction, and baseline subtraction via the use of OriginPro 9 software with a standard adjacent averaging smoothing method and a spline interpolation method. Center wavelengths were determined by fitting processed spectra to a Lorentzian function using MATLAB.

Quantification of ssCTTC$_3$TTC-(9,4) biodistribution ex vivo

ssCTTC$_3$TTC-(9,4) fluorescence from the liver, lung, heart, kidneys, and spleen was measured ex vivo using the instrument described in the preceding paragraph. Following acquisition, data was processed to apply spectral corrections for non-linearity of the InGaAs detector response, background subtraction, and baseline subtraction via the use of OriginPro 9 software with a standard adjacent averaging smoothing method and a spline interpolation method. The integrated intensity was then determined by calculating the area under the curve

from 1080-1180 nm with OrginPro 9 software. Integrated intensities were then normalized by dividing by the maximum value obtained for all measurements.

Fluorescence imaging of SWCNTs in vivo and ex vivo

Fluorescence imaging of SWCNTs in vivo and ex vivo was performed using a preclinical NIR hyperspectral mouse imaging system (Photon Etc.) (*49*). Excitation was provided by two continuous wave 730 nm diode lasers each with an output power of 2 W. Lasers were reflected off optical mirrors and distributed over the entire mouse with a maximum power density of 340 mW/cm^2. Emission light was filtered through an 1100 nm longpass filter to reduce autofluorescence. Intensity maps of SWCNT emission were produced by first creating a binary mask of images based off of intensity thresholding. For hyperspectral animal imaging, light was passed through a volume Bragg grating (VBG) as described in the "NIR hyperspectral microscopy of cells and resected tissue sections" section.

Analysis and processing of in vivo and ex vivo fluorescence images

In vivo hyperspectral cubes were processed as described in the section above titled "analysis and processing of hyperspectral data." In vivo and ex vivo fluorescence images were processed using ImageJ 1.48v. After image acquisition, background subtraction was performed using the "image calculator" function of ImageJ. Binary masks were then created via an intensity threshold method to excluded background noise from images. Masks were then multiplied by fluorescence images to produce intensity profiles which were overlaid on white light images.

Nanotube chirality and DNA sequence-dependent response to LDL

Sorted DNA-SWCNT samples were diluted to 0.2 mg/L in PBS and incubated with 0.5 mg/mL low-density lipoprotein (LDL, Alfa Aesar) for 6 hours at 37 degrees Celsius. Controls were incubated with no LDL present. Photoluminescent spectra were acquired with 0.5 second exposure time.

DNA-nanotube response to acidic pH

Phosphate buffered saline was mixed in a 1:1 ratio with a glacial-acetate buffer (final buffer strength was 10 mM) to allow a wide range of pH to be obtained. HCl and NaOH were used to titrate solutions at pH 5.4 and 7.2. Unsorted ssCTTC$_3$TTC-SWCNT was incubated in each solution for 18 hours at 37 degrees Celsius. Photoluminescent plots of DNA-SWCNT were then taken with a two second exposure time allowing ssCTTC$_3$TTC-(9,4) to be spectrally resolved.

Response of ssCTTC$_3$TTC-(9,4) to near saturating concentrations of biomolecules

ssCTTC$_3$TTC-(9,4) samples at a concentration of 0.4 mg/L were incubated in cell culture media (Dulbecco's modified Eagle media with 1% penicillin/streptomycin, and 1% glutamine) with 1% fetal bovine serum (Gibco) for 90 minutes at 37 degrees Celsius to allow for the acquisition of a protein corona. Samples were then mixed in a 1:1 ratio with bovine serum albumin (final concentration = 20 mg/mL), salmon testes dsDNA (final concentration = 1 mg/mL), or carboxymethyl cellulose (final concentration = 5 mg/mL). Samples were incubated for 18 hours at 37 degrees Celsius and spectra were taken with 730 nm excitation.

Titration of ssCTTC$_3$TTC-(9,4) with PEG-conjugated lipids

ssCTTC$_3$TTC-(9,4) samples at a concentration of 0.4 mg/L were incubated in cell culture media (Dulbecco's modified Eagle media with 1% penicillin/streptomycin, and 1% glutamine) with 1% fetal bovine serum (Gibco) for 90 minutes at 37 degrees Celsius to allow for the acquisition of a protein corona. Samples were then mixed in a 1:1 ratio with solutions of varying concentrations of lipids solubilized via conjugation with either polyethylene glycol (PEG) or methoxy-PEG, so that the final concentration of ssCTTC$_3$TTC-(9,4) in solution was 0.2 mg/L. The following PEG-conjugated lipids were used: Cholesterol-PEG 600, "PEG-Cholesterol", (Sigma Aldrich); C16 PEG750 Ceramide, "PEG-Ceramide", (Avanti Lipids); and 18:0 PEG550 PE, "mPEG-PE 18:0", (Avanti Lipids). Samples were incubated for 18 hours at 37 degrees Celsius. PEG and mPEG, with molecular weights of 600, 550, and 750 were used as controls to test for non-specific interactions. The concentrations of PEG and mPEG used matched the highest concentrations used for the PEG-lipid sensing experiment.

ssCTTC$_3$TTC-(9,4) response to U18666A, Lalistat 3a2, and imipramine in vitro

ssCTTC$_3$TTC-(9,4) was incubated at a concentration of 0.2 mg/L in complete cell culture media with 10% fetal bovine serum alone or with U18666A (3 μg/mL), Lalistat 3a2 (10 μM), or imipramine hydrochloride (10 μM) for 18 hours at 37 degrees Celsius. Spectra were then taken with 730 nm excitation as described previously.

Cell culture and reagents

RAW 264.7 TIB-71 cells (ATCC) were grown at 37 degrees Celsius and 5% CO_2 in sterile, filtered Dulbecco's modified Eagle media (DMEM) with 10% fetal bovine serum (heat inactivated) 2.5% HEPES, 1% glutamine, and 1% penicillin/streptomycin. For 100X imaging,

cells were plated on glass bottom petri dishes (MatTek). All cells were used at 70-80% confluence.

Reporter validation in live cells

Cells were treated with U18666A (3 μg/mL), Lalistat 3a2 (10 μM), or imipramine hydrochloride (10 μM) for 24 hours to allow for endolysosomal lipid accumulation to occur. Control cells were untreated. Following the 24 hour treatment period, nanotubes were added at 0.2 mg/L to fresh culture media and incubated with cells for 30 minutes at 37 degrees Celsius. Cells were then washed and media replaced to remove SWCNTs that had not been internalized during the 30 minute incubation. Data was acquired via NIR hyperspectral imaging 6 hours after SWCNT incubation.

Reporter response to HPβCD treatment in MEFs.

Mouse embryonic fibroblasts (MEFs) were incubated with the reporter and treated with U18666A (3 μg/mL) for 6 hours to induce endolysosomal lipid accumulation (*17*). Reporter emission wavelength was then measured via NIR hyperspectral imaging (*30*) (T=0). Following imaging, cells were treated with 150 μM of 2-(hydroxypropyl)-β-cyclodextrin (HPβCD) for twenty-four hours to remove lipids from endolysosomal organelles (*31*), or left untreated as controls. Reporter emission wavelength in the same plates of cells was once again measured via NIR hyperspectral imaging after the completion of the twenty-four hour treatment (or control) period (T=24).

Assessing the effect of ssCTTC$_3$TTC-(9,4) on lipoprotein hydrolysis.

RAW 264.7 macrophages were treated with 0.2 mg/L reporter (the in vitro working concentration) or PBS as a control. 3 hours later cells were treated with 50 μg/mL Alexa Fluor™-acetylated-low density lipoprotein (ThermoFisher) for 30 minutes. Following this 30 minute incubation cells were washed and fresh media was added. Cells were then washed 3 times with PBS and fixed with 4% paraformaldehyde immediately, or 3 hours after the addition of fresh media. Fluorescent images of cells were then taken using the FITC channel.

Molecular dynamics simulations

All-atom replica exchange molecular dynamics (REMD) simulations (*50-52*) were performed to understand the interactions between a carbon nanotube, single-stranded DNA, sphingomyelin, and cholesterol. Four strands of ssCTTC$_3$TTC DNA were placed in a desorbed state in the vicinity of a 4.757 nm long SWCNT with a (9,4) chirality. The DNA and SWCNT were solvated in a 5 x 5 x 4.757 nm water-box containing approximately 3,300 TIP3P model (*53*) water molecules and sodium counter-ions, placed randomly, to balance the negative charges from phosphates on DNA (fig. S6). The total system was ~11,500 atoms. The SWCNT extended to the edge of the water box. The SWCNT atoms were modeled as sp^2 hybridized carbon. All structures were visualized in VMD (*54*).

To run the REMD simulations, the Gromacs 4.6.7 simulation package was used with the Charmm36 force field. Long-range electrostatics were calculated using the particle mesh Ewald method with a 0.9 nm real space cutoff. For van der Waals interactions, a cutoff value of 1.2 nm was used. The DNA-SWCNT configuration was energy minimized and subjected to 100 ps equilibration (NVT) at 300 K. Forty replicas were created with temperatures ranging from 300 K to 585 K. Temperature intervals increased with absolute temperature to maintain uniform

exchange probability. The 40 replicas were run in parallel for 300 ns of NVT production. Exchange between adjacent temperature replicas was attempted every 2 ps and the temperature list was optimized to ensure that the acceptance ratio remained at least 20%. The time step of the simulation was 2 fs. The trajectories were saved every 10 ps, yielding a total of 30,000 snapshots for production analysis. For clustering, solvent accessibility, water density, and hydrogen bonding analysis, the 300 K trajectory was used.

Three molecules of sphingomyelin or 5 molecules of cholesterol (chosen to keep atom density approximately the same) were evenly distributed in the water-box of the top equilibrium cluster of the ssCTTC$_3$TTC + (9,4) configuration (fig. S6). This configuration served at the initial configurations for the combination simulations (DNA + sphingomyelin or DNA + cholesterol). The system was again energy-minimized, heated for 100 ps (NVT), and replicated in temperature space. The configurations were then run for an additional 200 ns of NVT production (hence 300 through 500 ns of total simulated time). Again, the 300 K trajectory was used for subsequent analysis. The simulation time totaled ([300 ns x 40] + 2*[200 ns x 40]) = 0.028 ms.

Clustering of the REMD trajectory is useful to determine the underlying equilibrium structures in the simulated configuration. Here, we used a native Gromacs clustering function (g_cluster) with a root mean square deviation (RMSD) cutoff of 0.8 nm based upon the positions of the DNA backbone atoms. The top cluster from the 30,000 available snapshots represented 21.4% of the total 300 K trajectory. We found significant inter-strand and intra-strand DNA interactions in the top cluster. In agreement with previous studies (*50, 51*), the DNA remained bound to the SWCNT throughout the duration of the simulation.

The solvent accessibility was analyzed using the Gromacs function 'g_sas'. In the ssCTTC$_3$TTC + (9,4) configuration, it was evident that the DNA evolved to wrap the SWCNT from its initially unbound state, and shield the SWCNT from solvent (water or sodium) molecules (fig. S7). The addition of the sphingomyelin or cholesterol molecules in the subsequent simulations further decreased the solvent accessibility to the SWCNT surface. Although the solvent accessibility to surface molecules decreased, there were significant changes in water density. This reflects the hydrophobic nature of sphingomyelin-water and cholesterol-water interfaces rather than steric constraint. This data is in agreement with a decrease in water density found near the surface of the SWCNT in the ssCTTC$_3$TTC + sphingomeylin + (9,4) and ssCTTC$_3$TTC + cholesterol + (9,4) configurations (Fig. 1).

Hydrogen bonding analysis was performed using the Gromacs function 'g_hbond'. In the ssCTTC$_3$TTC + (9,4) configuration, there was a significant increase in the number of DNA-DNA hydrogen bonds as the DNA adsorbed onto the SWCNT and adopted an equilibrium arrangement (fig. S7). Similar analyses were performed for the ssCTTC$_3$TTC + sphingomeylin + (9,4) and ssCTTC$_3$TTC + cholesterol + (9,4) configurations (fig. S7).

ssCTTC$_3$TTC-SWCNT removal from blood

ssCTTC$_3$TTC-SWCNT (200 μL of a 50 mg/L solution) was injected intravenously into male SKH1-Elite mice (6 weeks old) that were purchased from Charles River Laboratory. A higher concentration of SWCNT was used here to ensure signal could be seen within the circulation of the mice. SKH1 mice were used because their hairless nature aids in the imaging process. Immediately following injection, movies of mice were taken with the aforementioned preclinical mouse imaging system to determine the fluorescence intensity in different regions of

the mice. Images of mice were then taken periodically to quantify the fluorescence signal over the long term. Fluorescence intensity was quantified in three regions of interest (ROIs) for each mouse by drawing ROIs over white light images of the mice as shown in Figure 2.

Diet

"Western diet (WD)" mice were given an adjusted calorie diet ad libitum. This diet was purchased from Envigo (formerly Harlan Laboratories) and contained 42% calories from fat. By weight the diet contained 17.3% protein, 48.5% carbohydrate, 21.2% fat and 0.2% cholesterol (.05% from fat source, .15% added). Full details on the diet (TD88137) can be found here: http://dybiotech.skyd.co.kr/images/ath/88137.pdf. Water was supplemented with 42 g/L of high fructose corn syrup equivalent which consisted of 55% fructose and 45% glucose by weight (*55*). All other mice received standard chow and water ad libitum.

Tissue fixation and sectioning

Mouse organs were fixed in 10% buffered formalin phosphate and paraffin embedded before 5 µm sections were placed on glass slides. Paraffin was removed and the slides were stained with haematoxylin and eosin (H&E) for basic histology at the Molecular Cytology Core Facility of Memorial Sloan Kettering Cancer Center and Histowiz Inc. For frozen tissue sections a small piece of liver tissue was placed in an optical cutting temperature (OCT, Tissue-Tek) formulation for ten minutes and then transferred to a mold containing OCT. The mold with tissue was then placed into a stainless steel beaker of 2-methylbutane that has been cooled in liquid nitrogen. After the OCT had solidified completely, the block was removed from the 2-methylbutane and placed on dry ice or in a -20°C cryostat. Five micron sections were placed on

glass slides. Thirty minutes later slides were washed with phosphate buffered saline. Finally slides were covered with a cover slip and then imaged.

Transmission electron microscopy

Liver tissue was rinsed with PBS and then cut into ~5 mm cubes. Cubes were placed in a modified Karnovsky's fix of 2.5% glutaraldehyde, 4% parafomaldehye and 0.02% picric acid in 0.1M sodium caocdylate buffer for sixty minutes. Following a secondary fixation in 1% osmium tetroxide, 1.5% potassium ferricyanide, samples were dehydrated through a graded ethanol series, and embedded in an epon analog resin. Ultrathin sections were cut (55-60 nm) using a Diatome diamond knife (Diatome) on a Leica Ultracut T ultramicrotome (Leica Microsystems). Sections were then placed on copper grids, contrasted with lead citrate and viewed on a JEM 1400 electron microscope (JEOL) operated at 100 kV. Images were recorded with a Veleta 2K x 2K CCD camera (Olympus-SIS).

Atomic force microscopy

A stock solution (2.5 mg/L in PBS) of ssCTTC$_3$TTC-(9,4) was diluted 1:5 in a buffer consisting of 20 mM HEPES (pH 6.8) and 5 mM $MgCl_2$. 40 µl of this solution was plated on freshly cleaved mica substrate (SPI) for ~30 minutes before washing with 10 mL of Molecular Biology Grade H_2O (Fisher BP2819-1) and blown dry with nitrogen gas. Imaging was performed using a Cypher S AFM (Asylum Research), with an Olympus AC240TS-R3 AFM probe (Asylum Research) in tapping mode at room temperature. Images were captured for length distribution measurements at a scan size of 2µm x 2µm (1024 x 1024), as well as an overview image at 6µm x 6µm (2048 x 2048).

Quantification of steatotic area in hepatic tissue sections

Images of tissue sections stained with hematoxylin and eosin (H&E) were analyzed to quantify the steatotic/lipid rich area visible in each field of view, denoted by white/clear areas corresponding to lipid droplets. Images were manually cropped to remove areas that did not contain tissue. The H&E images, which are RGB, were deconvolved into three 8-bit constituent color components using the FIJI Color Deconvolution Plug-in (*56*). The second color component was thresholded (220 to 225 intensity units) to obtain a binary mask. This binary image was analyzed to select regions of interest (ROI, no constraint on shape but a minimum size of 20 pixels^2) representing lipid droplets. Areas that were identified as blood vessels, or other non-steatotic white area on tissue sections were manually removed. A 'steatotic fraction of imaging area' for each image was obtained by combining the area of the lipid droplets and dividing by the total area of the image.

Hepatic cell isolation

C57BL/6 mice were purchased from Jackson Laboratories, at age 6-8 weeks of age. Mouse hepatocytes were harvested via a two-step in situ collagenase perfusion technique modified from Seglen. Briefly, mice were anesthetized using isofluorane. The portal vein was cannulized, and in vivo perfusion (5 mL/min X 10 min) was performed with a calcium-free hydroxyethylpiperazineethanesulfonic acid (HEPES)-buffered solution (143 mM NaCl, 6.7 mM KCl, 10 mM HEPES, 100 mg% ethylene glycol-bis-aminoethyl ether (EGTA; Sigma, St. Louis, MO), pH 7.4), and then perfused (5 mL/min X 10 min) with a second HEPES-buffered solution (67 mM NaCl, 6.7 mM KCl, 4.8 mM CaCl, 100 mM HEPES, 1.0 g bovine albumin (Sigma), pH

7.6) containing 0.05% collagenase D (Roche Corp.). The liver was then resected and placed in isolation medium [Williams' E medium (GIBCO) with 10,000 U/liter penicillin G, 100 mg/liter streptomycin sulfate]. The liver capsule was peeled back from all lobes, and the liver was then gently combed to isolate hepatocytes. The hepatocyte pellet was resuspended in isolation medium following gauze filtration and centrifuged at 50 g for 10 minutes. The cells were then resuspended and placed on top of Percoll gradient and hepatocyte fraction was isolated. The nonparenchymal cell fraction was further processed. F4/80 labeling was completed and the F4/80 positive population was sorted and plated down on tissue culture treated plastic for further analysis.

HSC were isolated using in situ digestion protocol as described in (*57*). In brief pronase/collagenase perfusion of mouse liver was performed with subsequent in vitro digestion; and density gradient–based separation of HSCs from other hepatic cell populations. FACS was then performed to ensure HSC purity by obtaining the Violet bright population.

NIR hyperspectral imaging and analysis of sensor uptake in isolated hepatic cells

Kupffer cells and hepatocytes were isolated from C57BL/6 mice that were injected intravenously with ssCTTC$_3$TTC-SWCNT as described in the section above entitled "Hepatic cell isolation." Transmitted light, NIR broad-band and NIR hyperspectral images were obtained from cells and emission in each image was summed from 1100-1300 nm to calculate the total near-infrared emission from each pixel in an image. For each cell we calculated the mean nanotube emission intensity per cell, and normalized this to the average nanotube emission intensity in Kupffer cells as these cells exhibited the highest amount of SWCNT uptake. To assess SWCNT uptake in hepatic stellate cells C57BL/6 mice were injected with ssCTTC$_3$TTC-SWCNT and their livers

pooled to allow for isolation of hepatic stellate cells as described in the section above entitled "Hepatic cell isolation." Imaging was performed on hepatic stellate cells as described above. For comparison, imaging was also performed on unsorted hepatic cells from the same mice. In total, hyperspectral images were taken of forty-eight individual cells (which all had morphologies and SWCNT uptake similar to what was seen in the sorted Kupffer cell images) present in the unsorted cell mixture that exhibited SWCNT uptake. To control for potential differences in the tail vein injections, the SWCNT intensity from within hepatic stellate cells was normalized by the intensity of the cells in the unsorted plate that showed SWCNT uptake. This normalized intensity per cell is presented in Figure 2E.

Testing for the interference of circulating lipids in whole blood

To determine whether the reporter was affected by the concentration of circulating lipids in mice, we tested its response against elevated cholesterol concentration in whole blood. Blood was removed from S.C. or W.D. mice after three months of feeding. The reporter was incubated in whole blood for three hours at 37 °C with constant mixing. Based on previous experiments, this incubation time is considerably longer than the time the reporter spends in the circulation (Fig. 2A). After this incubation period, the reporter emission wavelength was measured.

Assessing hepatic gene expression following reporter injection

Mice were injected with 200 ng of ssCTTC$_3$TTC-(9,4) (the in vivo working concentration) or PBS as a control. RNA was then isolated from the livers of mice 12, 24, or 72 hours post injection and RT-qPCR was performed to assess changes in the expression of *Ifnα, Ifnβ1, Il-6, Il-10, Il-28a, Il-28b, Il-29, Il-8, Tnfα, Tgfβ1, Cxcl10*, and *Isg15***.**

.

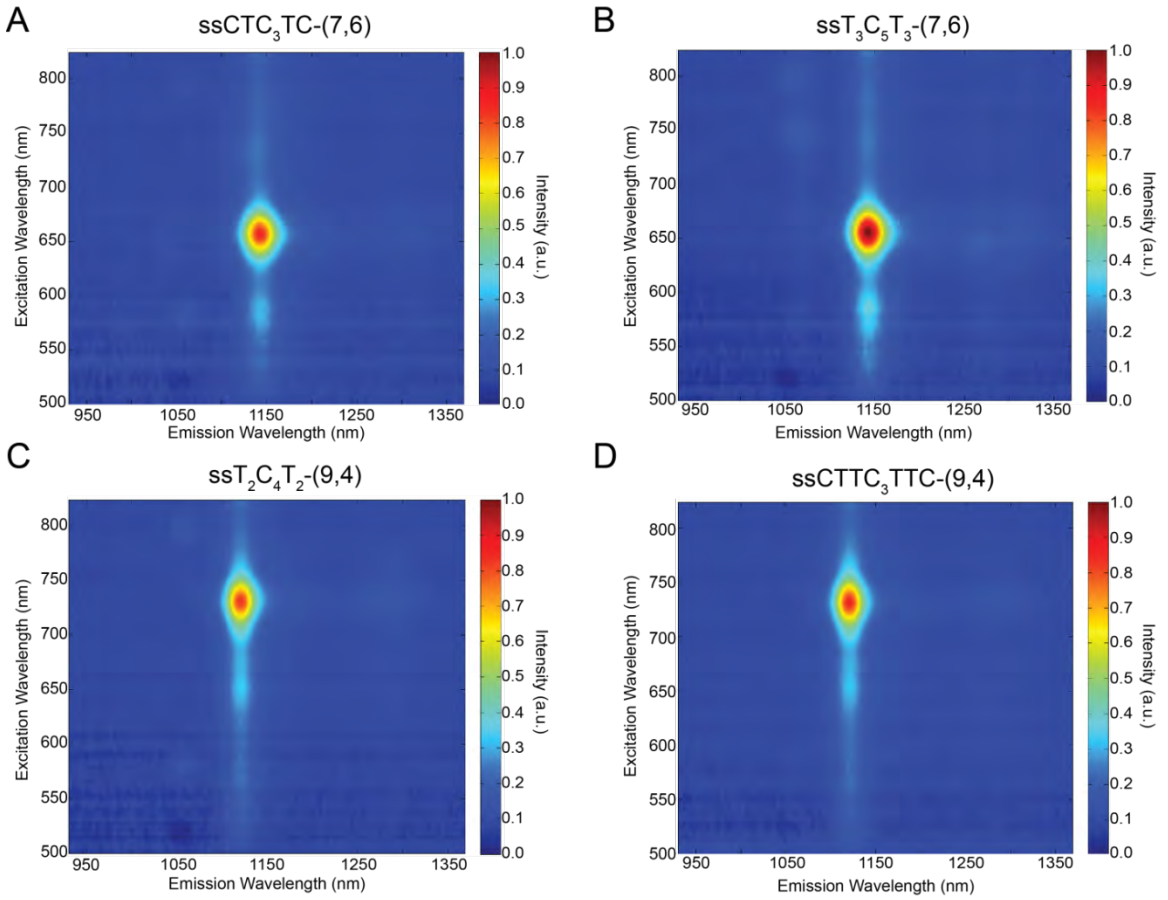

Fig. S1. Two-dimensional photoluminescence (PL) plots of isolated SWCNT chiralities. (A) PL plot of the (7,6) SWCNT non-covalently complexed with ssCTC$_3$TC. **(B)** PL plot of the (7,6) SWCNT non-covalently complexed with ssT$_3$C$_5$T$_3$. **(C)** PL plot of the (9,4) SWCNT non-covalently complexed with ssT$_2$C$_4$T$_2$. **(D)** PL plot of the (9,4) SWCNT non-covalently complexed with ssCTTC$_3$TTC.

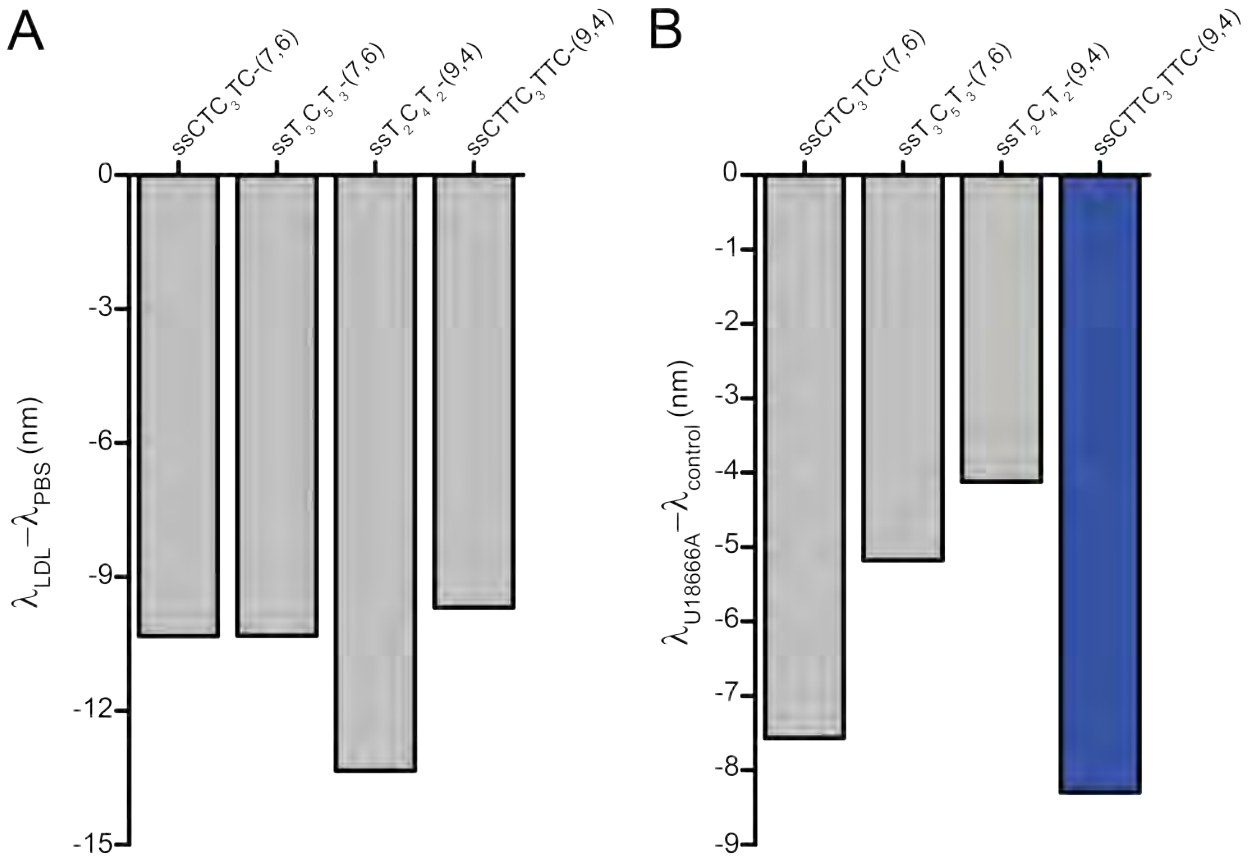

Fig. S2. Identification of ssCTTC$_3$TTC-(9,4) as a potential probe for endolysosomal lipid accumulation. (A) Photoluminescent response of DNA-nanotube complexes to 0.5 mg/mL low density lipoprotein in solution following a 6 hour incubation at 37 degrees Celsius. **(B)** Emission wavelength of ssCTTC$_3$TTC-(9,4) in RAW 264.7 macrophages cultured in the presence of U18666A (3 μg/mL for twenty-four hours) to force endolysosomal lipid accumulation compared to the emission wavelength seen from untreated control cells.

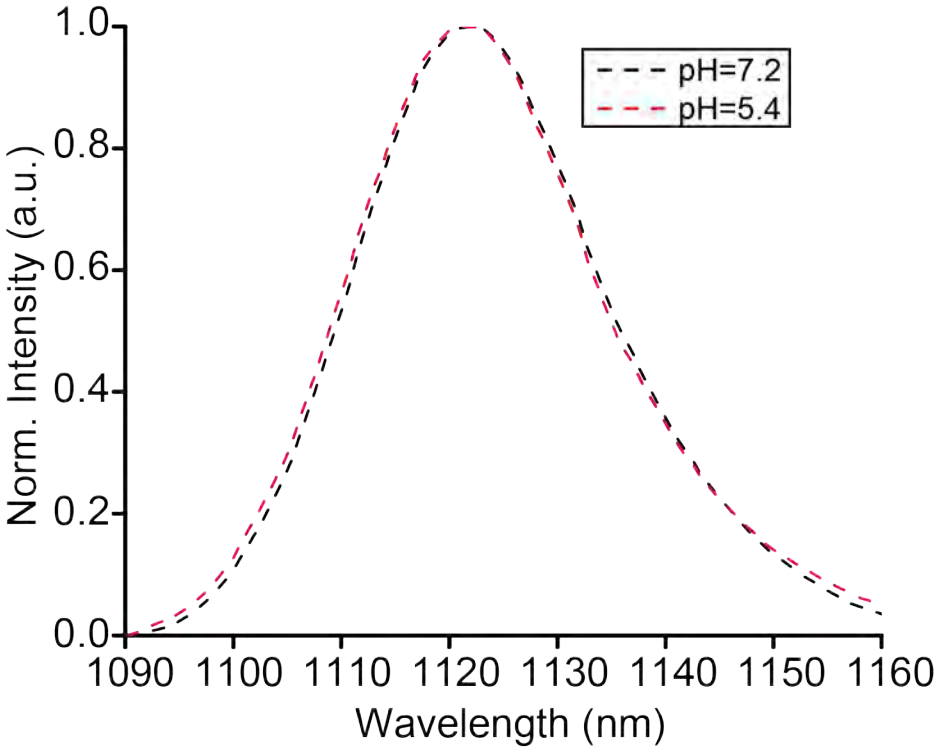

Fig. S3. Representative emission spectra of ssCTTC$_3$TTC-(9,4) at a neutral and acidic pH.

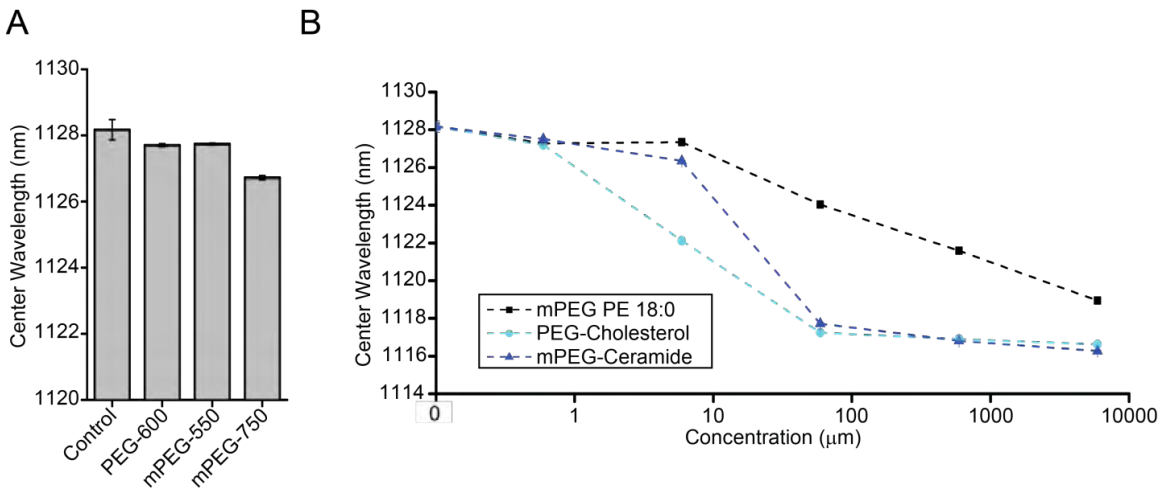

Fig. S4. ssCTTC$_3$TTC-(9,4) photoluminescent response in solution. (A) Mean emission wavelength of ssCTTC$_3$TTC-(9,4) in response to PEG and mPEG molecules. Concentrations of PEG/mPEG represented here are equal to the concentrations of PEG/mPEG used to solubilize the PEGylated lipids represented in Fig. 1. **(B)** Photoluminescent response of ssCTTC$_3$TTC-(9,4) to increasing concentrations of PEG-cholesterol, mPEG-ceramide and mPEG-phosphoethanolamine 18:0 (mPEG-PE 18:0). Error bars represent standard deviation from N=3 technical replicates.

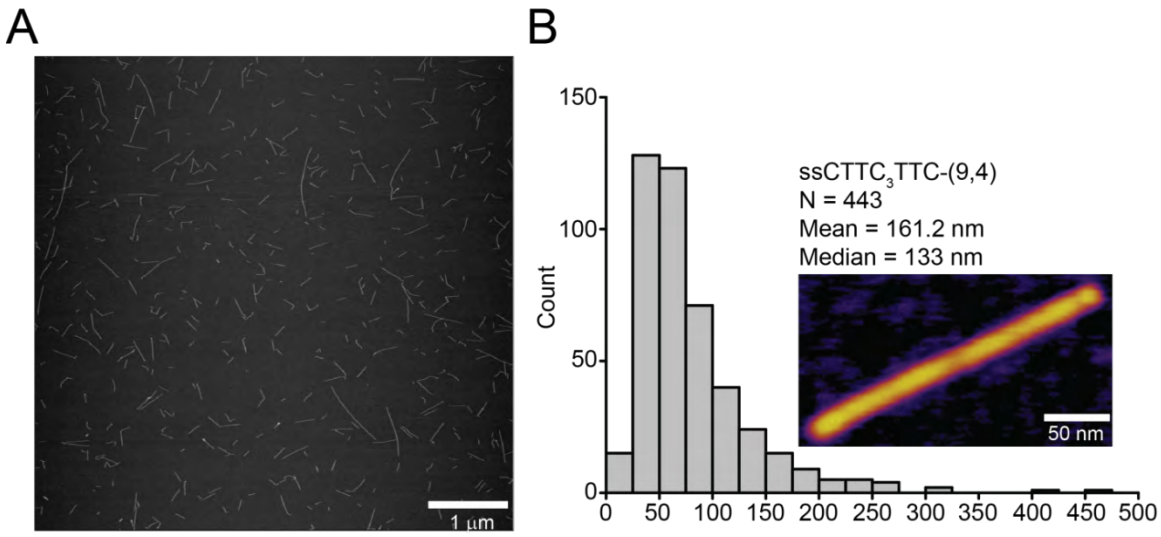

Fig. S5. Atomic force microscopy (AFM) of ssCTTC$_3$TTC-(9,4) complexes. (A) AFM image of ssCTTC$_3$TTC-(9,4) deposited on a surface. **(B)** Length distribution of ssCTTC$_3$TTC-(9,4) as quantified from AFM images, with a high resolution image of an ssCTTC$_3$TTC-(9,4) complex (inset).

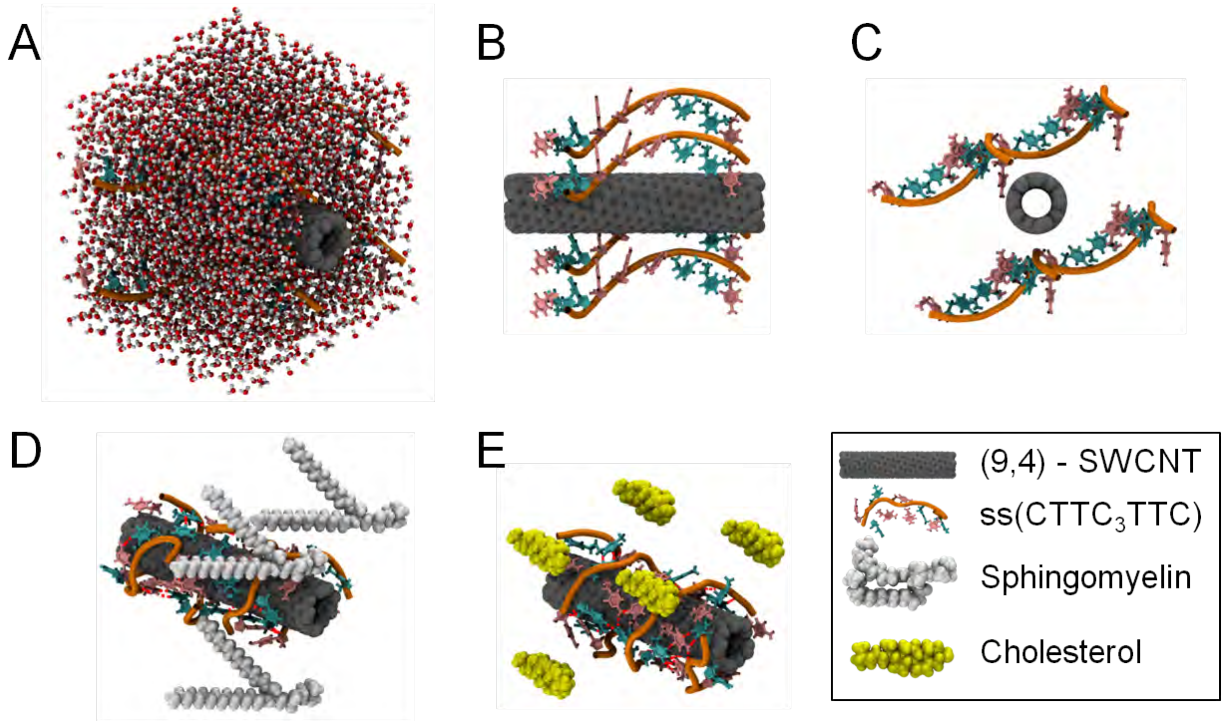

Fig. S6. Initial replica exchange molecular dynamics (REMD) configurations. (A) Starting configuration of the ssCTTC$_3$TTC DNA oligonucleotide with the (9,4) nanotube species shown in an explicit water box with counter-ions. **(B)** Side view of the ssCTTC$_3$TTC + (9,4) nanotube shown with water and ions removed. **(C)** Similar configuration shown edge-on. **(D)** Starting configuration of the ssCTTC$_3$TTC-(9,4) nanotube complex in the presence of sphingomyelin. **(E)** Similar starting configuration in the presence of cholesterol.

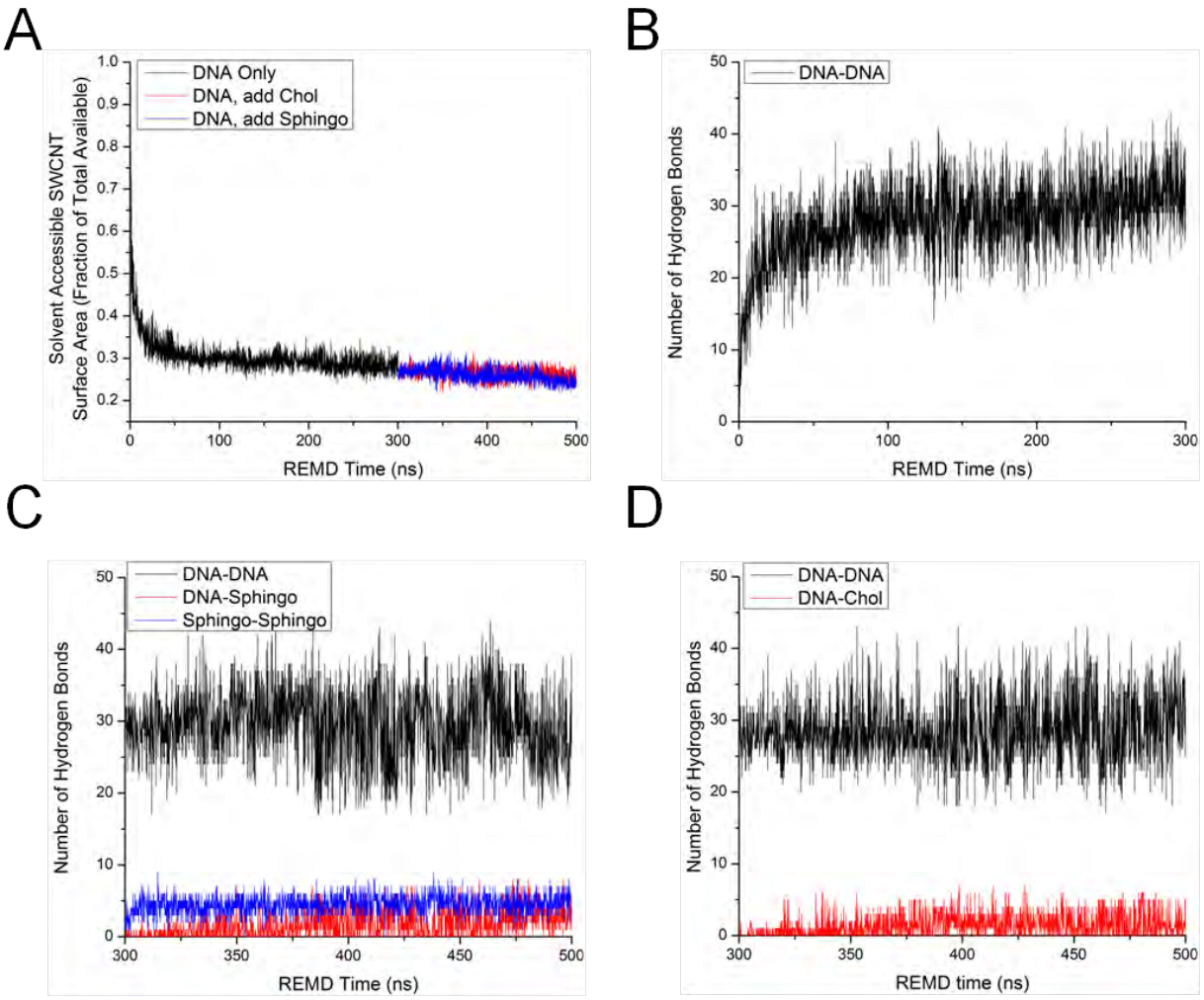

Fig. S7. Analysis of REMD simulations. (A) Solvent-accessible SWCNT surface area vs. simulation time for the three simulated configurations (DNA only, DNA + cholesterol, and DNA + sphingomyelin). **(B)** Number of hydrogen bonds between DNA strands vs. simulation time for the ssCTTC$_3$TTC + (9,4) configuration. **(C)** Number of DNA-DNA, DNA-sphingomyelin, and sphingomyelin-sphingomyelin hydrogen bonds in the ssCTTC$_3$TTC-(9,4) nanotube + sphingomyelin configuration. **(D)** Similar hydrogen bond analysis for the ssCTTC$_3$TTC-(9,4) nanotube + cholesterol configuration.

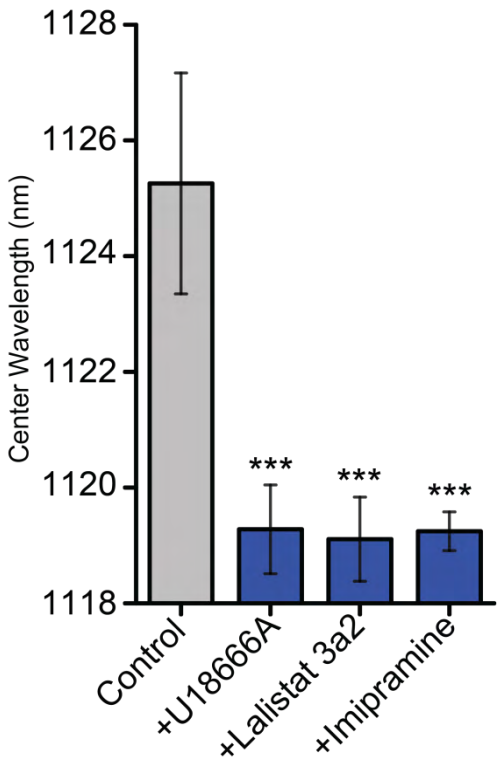

Fig. S8. Mean emission wavelength of ssCTTC$_3$TTC-(9,4) in live RAW 264.7 macrophages treated with inhibitors. Cells were treated with U18666A (3 μg/mL), Lalistat 3a2 (10 μM), or imipramine hydrochloride (10 μM) for twenty-four hours. *** = $P < 0.001$ compared to control, one-way ANOVA with Dunnet's multiple comparison test (N=7 for control, 3 for all other groups). Error bars represent standard deviation.

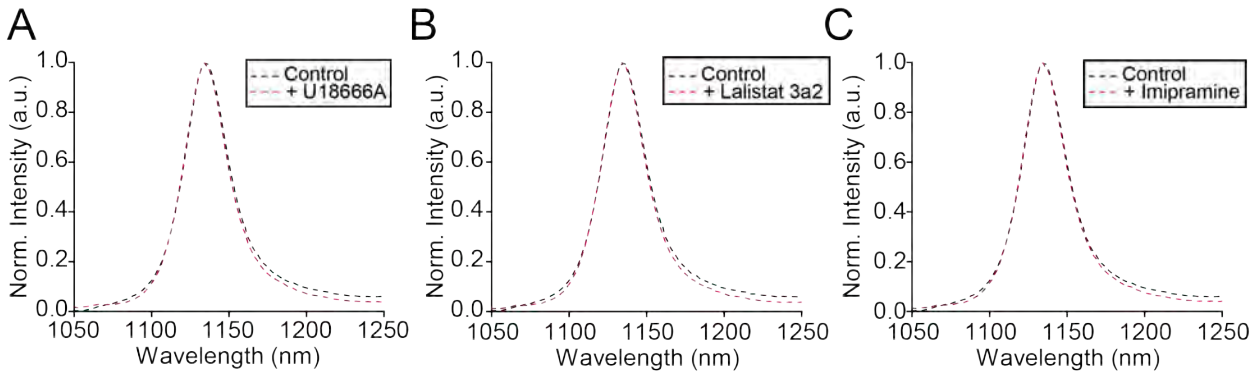

Fig. S9. Effect of inhibitors on ssCTTC$_3$TTC-(9,4) emission spectra in solution. (A) Representative emission spectra of ssCTTC$_3$TTC-(9,4) in solution alone and after incubation with 3 µg/mL U18666A at 37 degrees Celsius for eighteen hours. **(B)** Representative emission spectra of ssCTTC$_3$TTC-(9,4) in solution alone and after incubation with 10 µM Lalistat 3a2 at 37 degrees Celsius for eighteen hours. **(C)** Representative emission spectra of ssCTTC$_3$TTC-(9,4) in solution alone and after incubation with 10 µM imipramine hydrochloride at 37 degrees Celsius for eighteen hours.

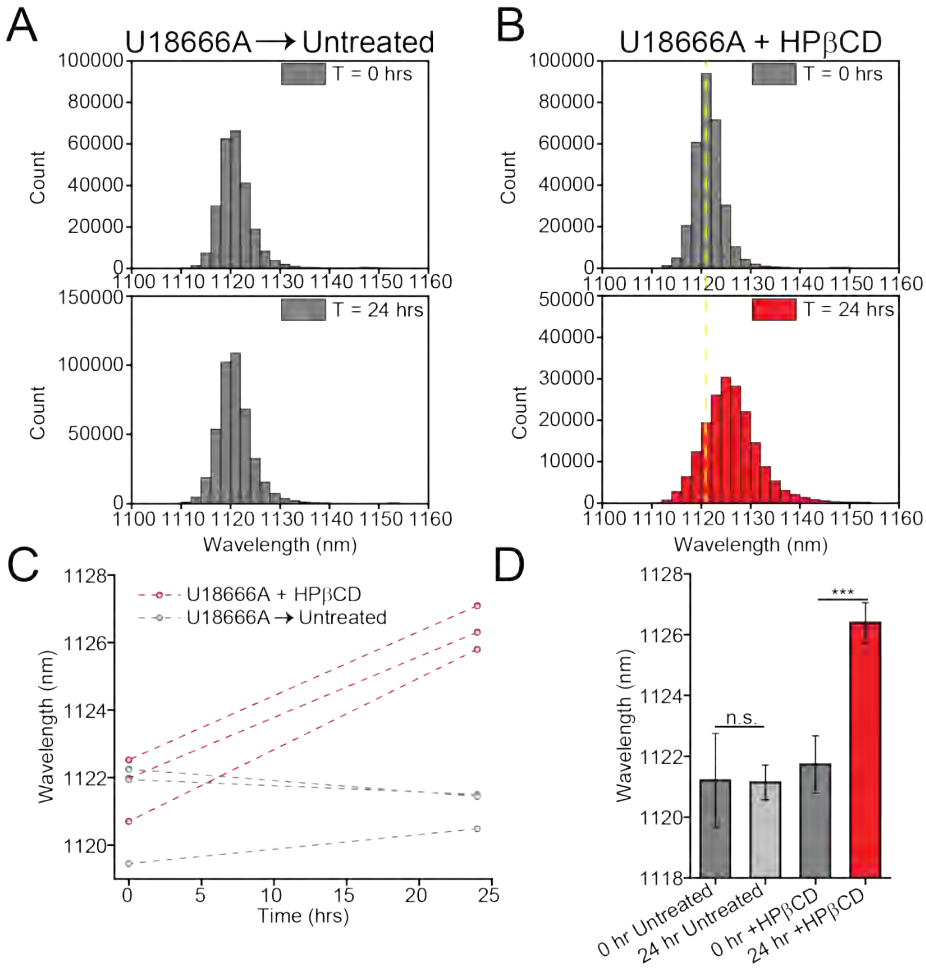

Fig. S10. Reporter response to HPβCD treatment in MEFs. (A) Histogram of emission center wavelengths from all pixels with NIR emission from hyperspectral images of cells treated with U18666A for six hours, and then left untreated at T=0 hrs and T=24 hrs. **(B)** Histogram of emission center wavelengths from all pixels with NIR emission from hyperspectral images of cells treated with U18666A for six hours, and then HPβCD at T=0 hrs and T=24 hrs of HPβCD treatment. **(C)** Mean reporter emission wavelength from U18666A treated plates of cells before and after further treatment with HPβCD (or untreated, time matched controls). **(D)** Mean reporter emission wavelength in MEFs that were treated with U18666A for 6 hours and then treated with HPβCD for 24 hours, or left untreated as controls. *** = $P < 0.001$ as measured with a one-way ANOVA with Sidak's post test. N=3 plates per condition.

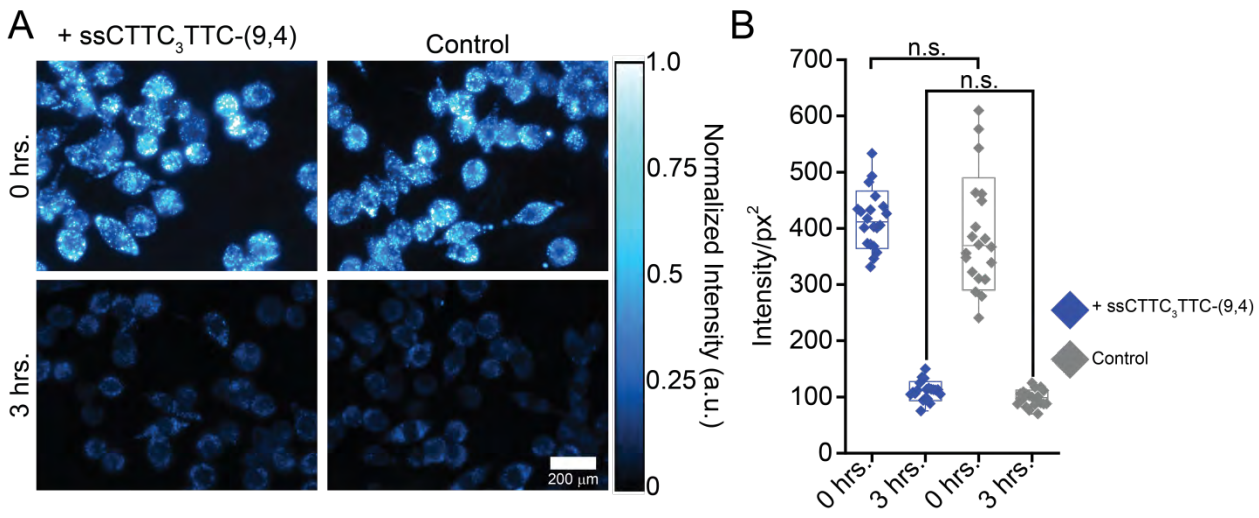

Fig. S11. Assessing the effect of ssCTTC3TTC-(9,4) on lipoprotein hydrolysis. (A) Representative epifluorescence images of Alexa 488-acLDL (blue) in RAW 264.7 macrophages, at 0 and 3 hours after the addition of acLDL in both reporter and PBS treated cells. **(B)** Fluorescence intensity per pixels^2 (px^2). N=20 twenty images per condition were analyzed. Data were compared using a one-way ANOVA with Sidak's multiple comparison test (n.s. = not significant).

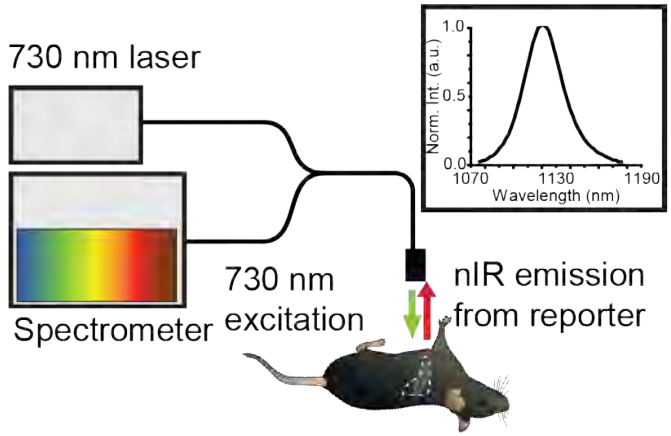

Fig. S12. Near-infrared in vivo spectroscope. Schematic of the near-infrared, in vivo spectroscope used for the non-invasive detection of ssCTTC$_3$TTC-(9,4) from the liver in vivo. A spectrum obtained after intravenous injection with 200 ng ssCTTC$_3$TTC-(9,4) is shown in the inset.

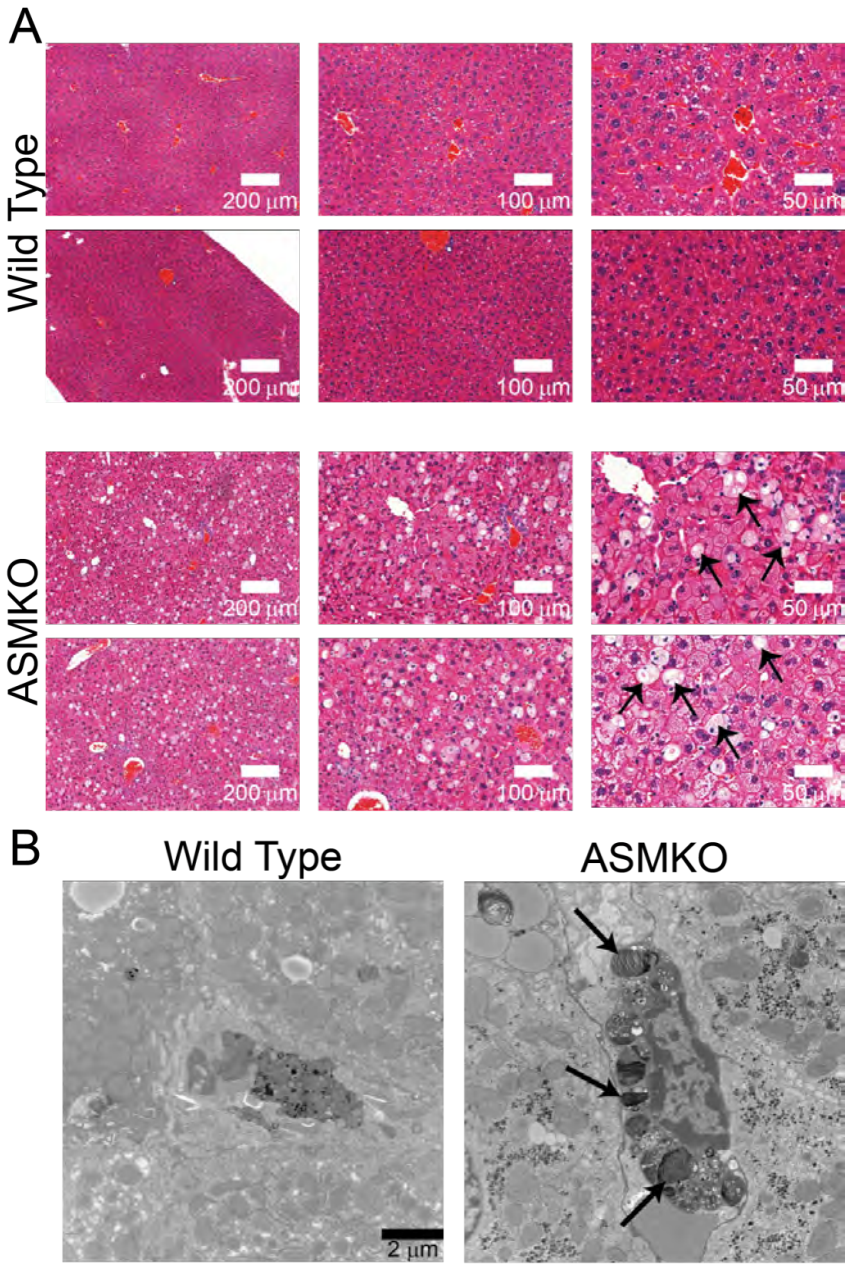

Fig. S13. Representative images of liver tissue from wild type and acid sphingomyelinase knockout (ASMKO) mice. (A) Representative images of H&E stained tissues from the livers of wild type and ASMKO mice. Arrows denote "foamy" cells in ASMKO livers. **(B)** Representative transmission electron microscopy (TEM) images of liver tissues showing Kupffer cells from wild type and ASMKO mice. Note the lipid-laden lysosomes (arrows) in the Kupffer cell of an ASMKO mouse. Representative images were chosen from N=3 mice per group.

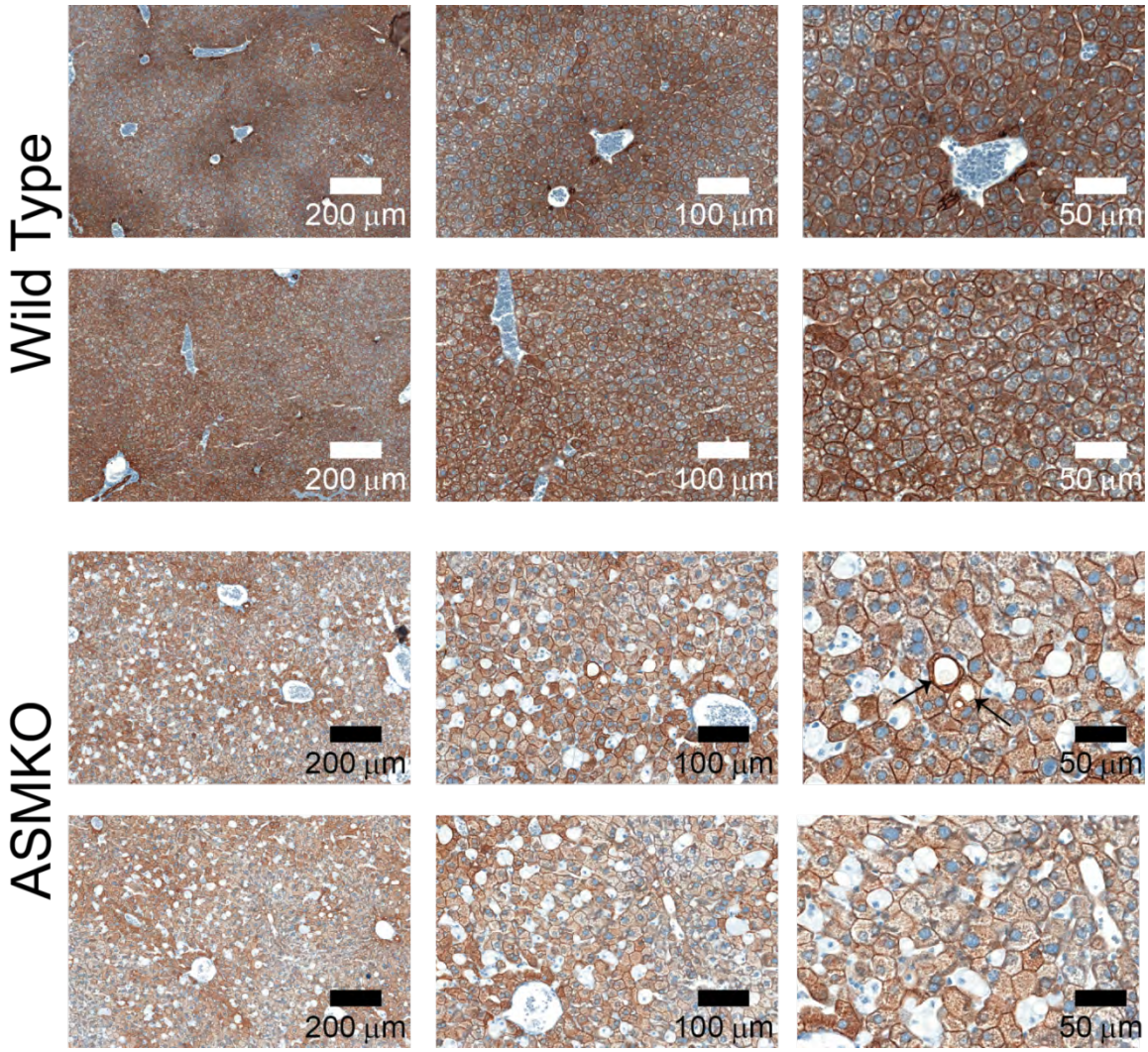

Fig. S14. Representative images of hepatic tissues from wild type and ASMKO mice stained with the hepatocyte marker CK8/18. Arrows indicate lipid-laden (foamy) hepatocytes (marked in brown). Representative images were chosen from N=3 mice per group.

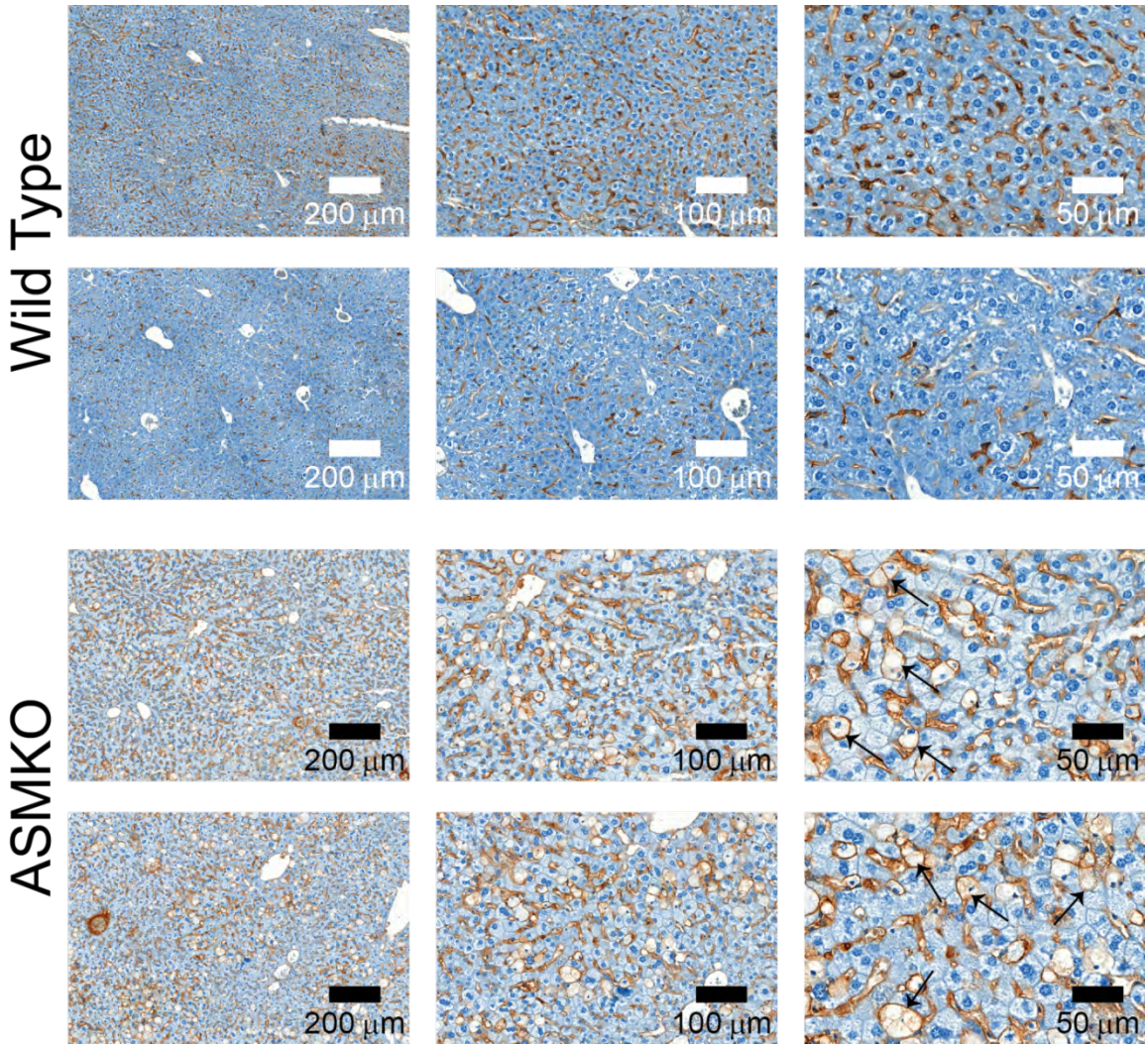

Fig. S15. Representative images of hepatic tissue from wild type and ASMKO mice stained with the Kupffer cell marker F4/80. Arrows indicate lipid-laden (foamy) Kupffer cells (marked in brown). Representative images were chosen from N=3 mice per group.

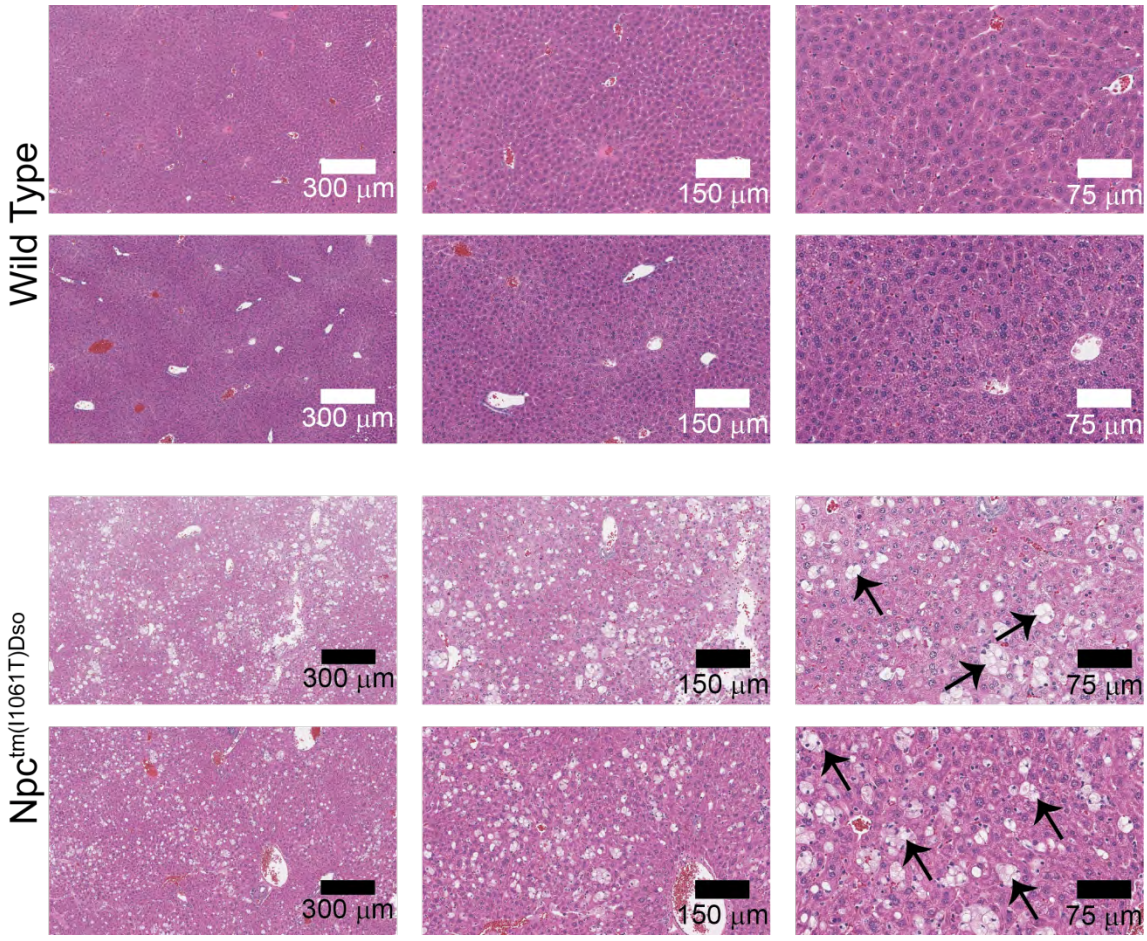

Fig. S16. Representative images from H&E-stained tissues from the livers of wild type and Npctm$^{(I1061T)Dso}$ mice. Arrows denote "foamy" cells in Npc$^{tm(I1061T)Dso}$ livers. Representative images were chosen from N=3 mice per group.

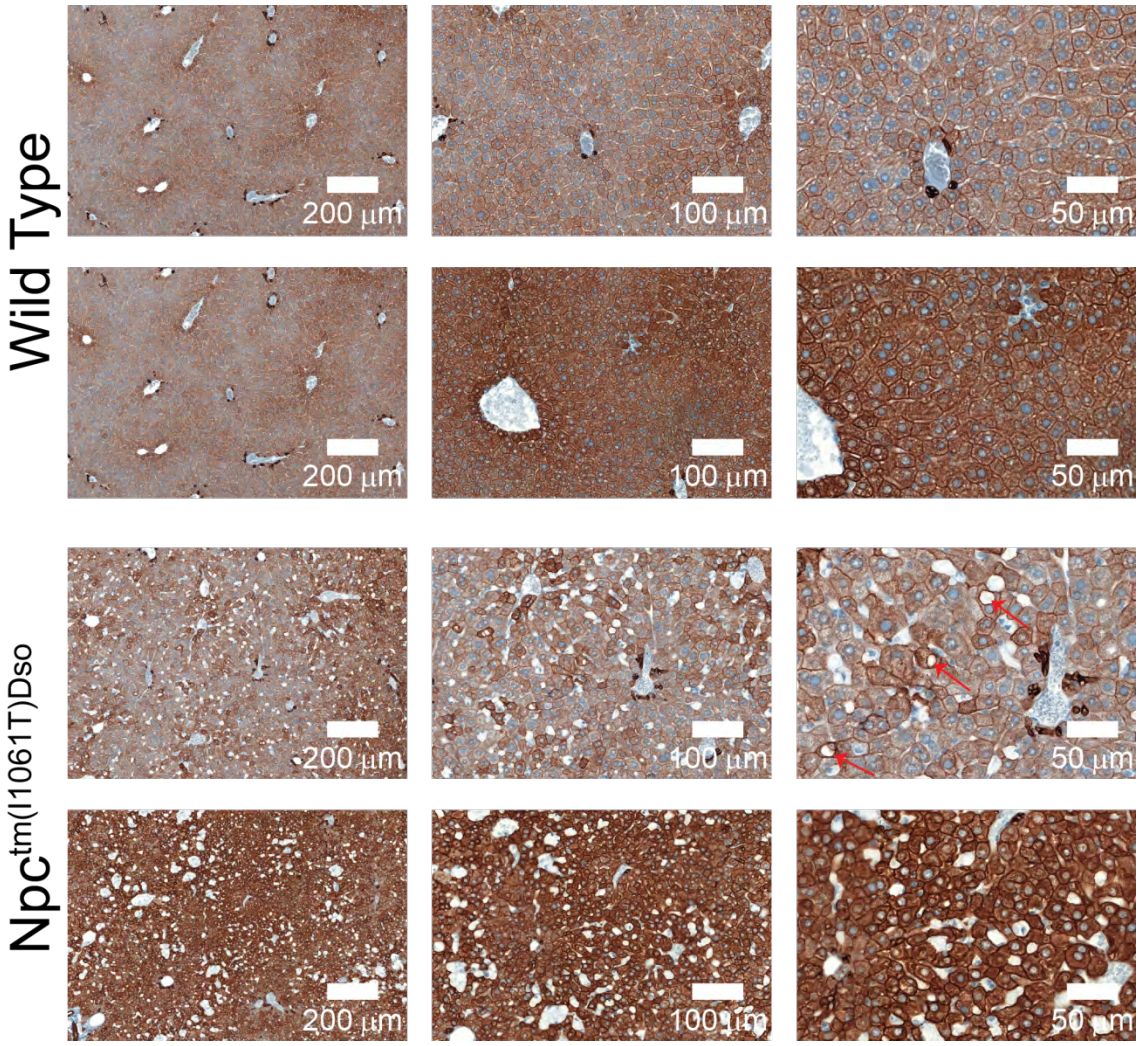

Fig. S17. Representative images of hepatic tissue from wild type and Npctm$^{(I1061T)Dso}$ mice stained with the hepatocyte marker CK8/18. Arrows indicate lipid-laden (foamy) hepatocytes (marked in brown). Representative images were chosen from N=3 mice per group.

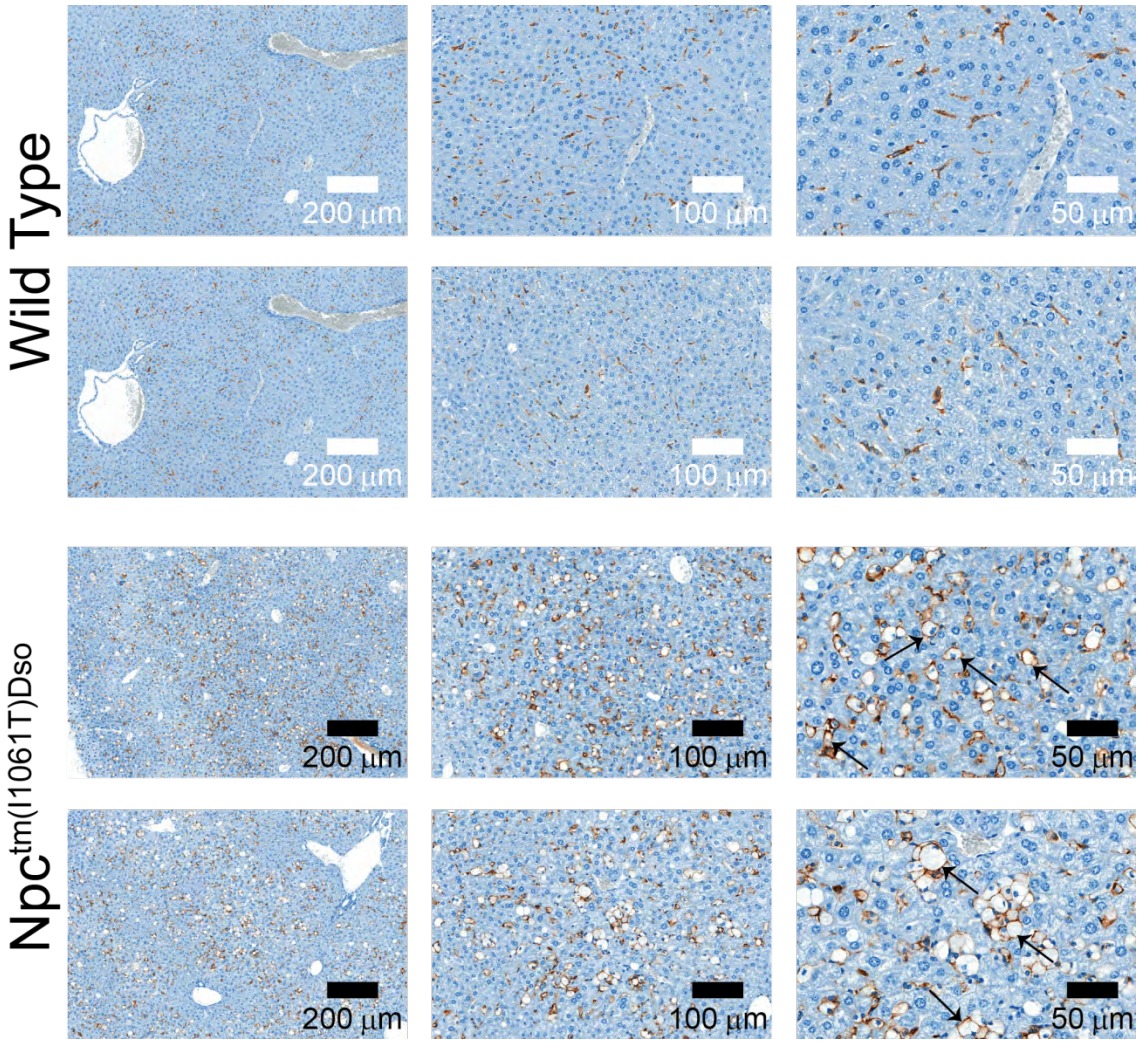

Fig. S18. Representative images of hepatic tissues from wild type and Npctm(I1061T)Dso mice stained with the Kupffer cell marker F4/80. Arrows indicate lipid-laden (foamy) Kupffer cells (marked in brown). Representative images were chosen from N=3 mice per group.

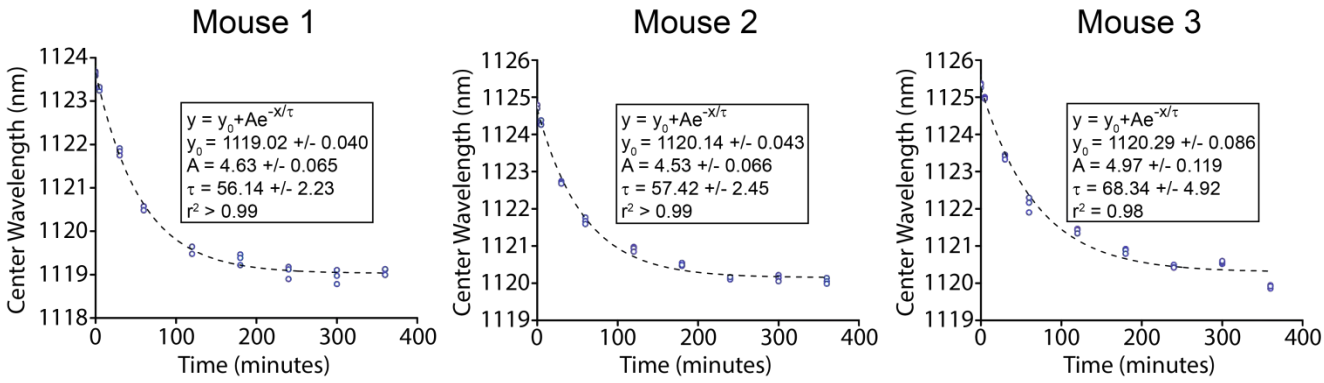

Fig. S19. Exponential fits of the decrease in ssCTTC$_3$TTC-(9,4) emission wavelength following intravenous injection of 200 µg of oxLDL in mice. Fits are shown for three biological replicates, with multiple technical replicates taken for each time point.

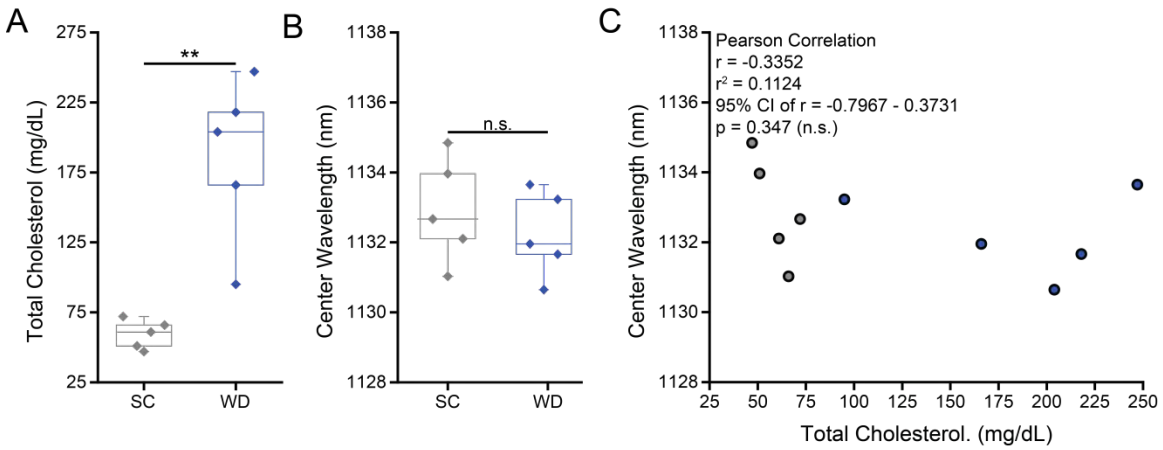

Fig. S20. Testing the effects of elevated lipid concentrations on reporter emission in whole blood. (A) Serum cholesterol concentrations of mice fed standard chow (SC) or the Western Diet (WD) for 3 months. **(B)** Reporter emission center wavelength after incubating for three hours in whole blood collected from the SC and W.D mice in (A). **(C)** Reporter emission center wavelength measurements collected after incubation in whole blood with the specified total cholesterol concentrations. The 95% confidence interval of the Pearson correlation coefficient (r) ranged from -0.7967 – 0.3731 indicating that no statistically significant correlation was observed between reporter emission center wavelength and blood cholesterol concentrations.

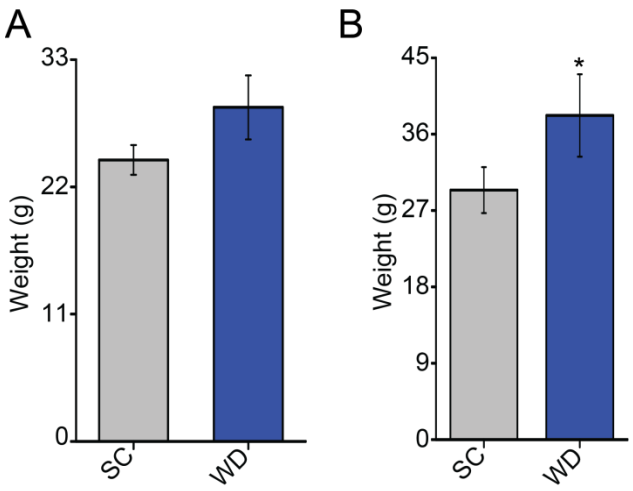

Fig. S21. Weights of male C57BL/6 mice fed SC or the Western diet with HFCS. (A) Weights of SC and WD mice after one month of feeding. **(B)** Weights of SC and WD mice after three months of feeding. * = $P < 0.05$ determined with a t-test with Welch's correction. Error bars represent standard deviation. N=3-4 per group mice for panel A, N=5 mice per group for panel B.

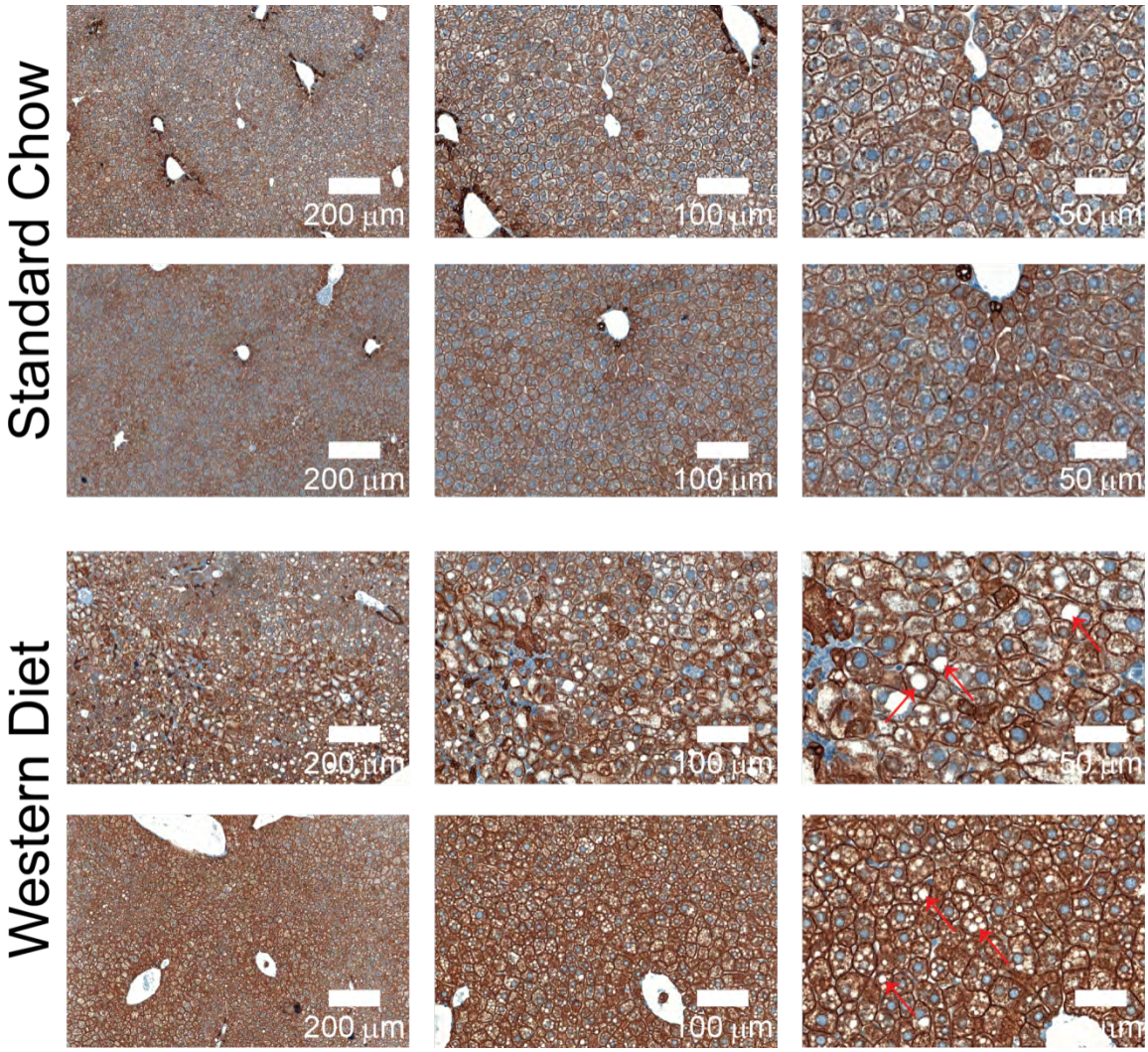

Fig. S22. Representative images of hepatic tissues stained with CK8/18 from mice fed SC or the WD with HFCS for one month. Arrows indicate lipid-laden hepatocytes which are marked with CK8/18 (brown). Representative images were chosen from N=3-4 mice per group.

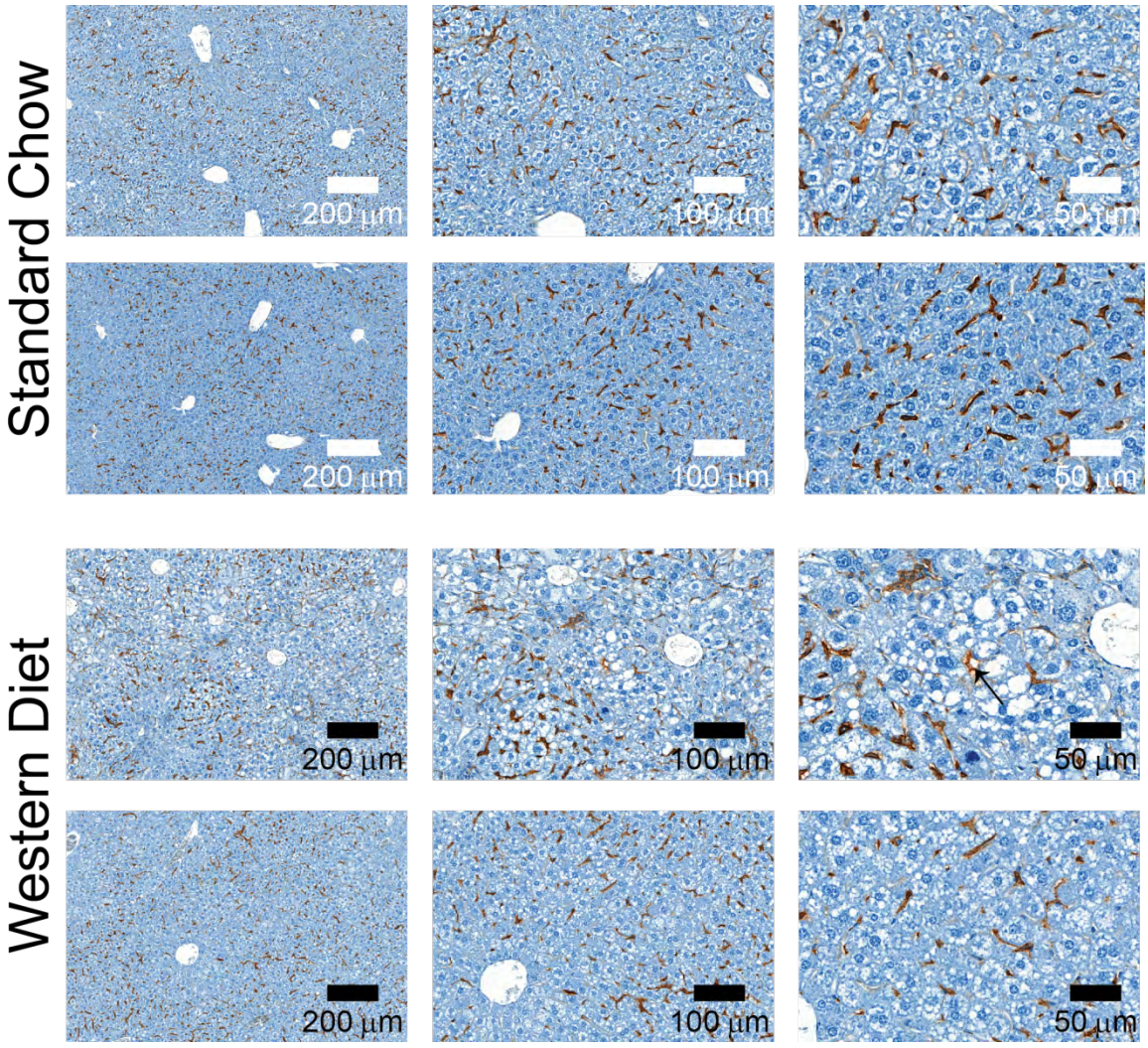

Fig. S23. Representative images of hepatic tissues stained with F4/80 from mice fed SC or WD with HFCS for one month. Arrows indicate lipid-laden Kupffer cells which are marked with F4/80 (brown). Representative images were chosen from N=3-4 mice per group.

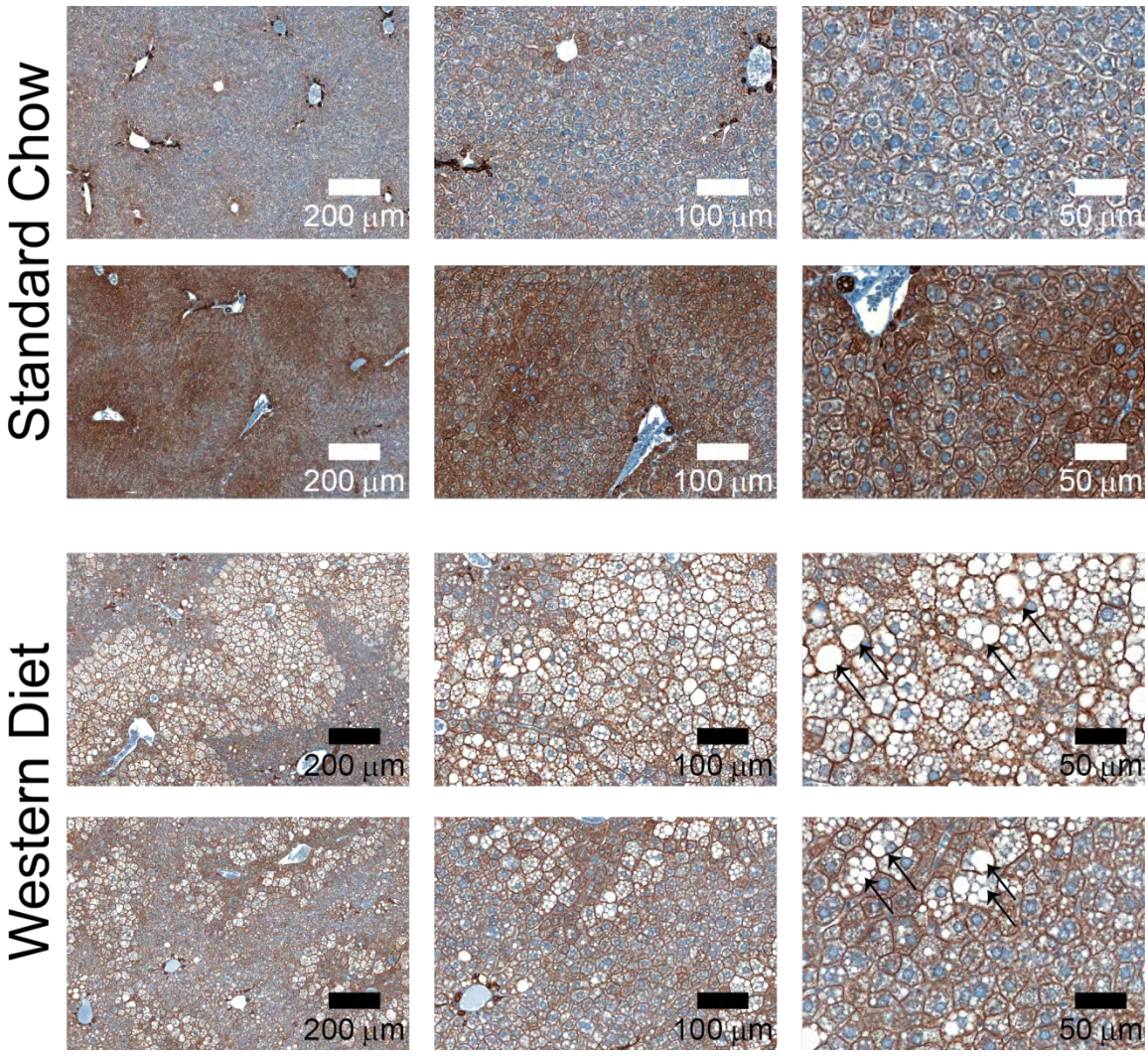

Fig. S24. Representative images of hepatic tissues stained with CK8/18 from mice fed SC or the WD with HFCS for three months. Arrows indicate lipid-laden hepatocytes which are marked with CK8/18 (brown). Representative images were chosen from N=5 mice per group.

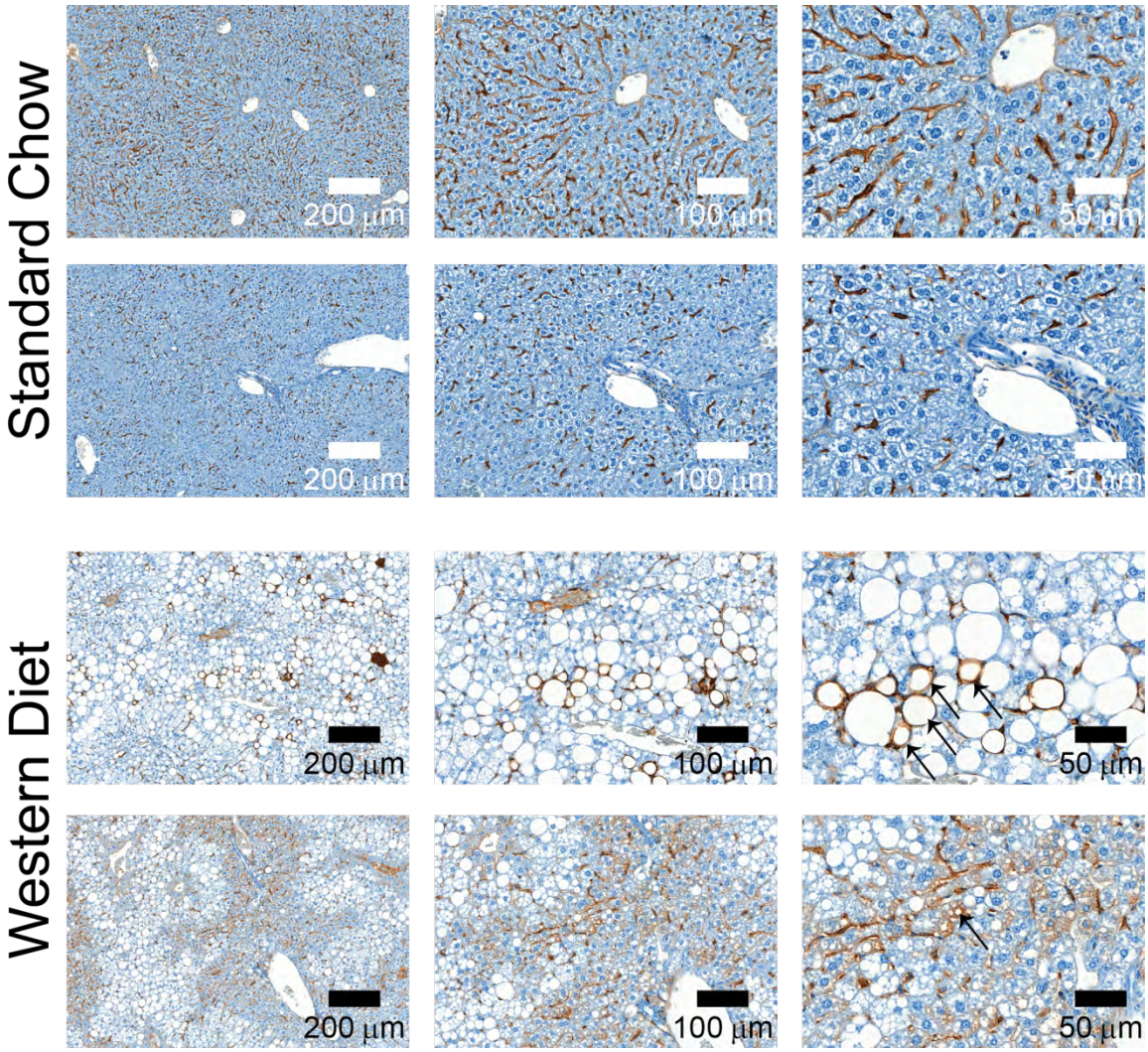

Fig. S25. Representative images of hepatic tissues stained with F4/80 from mice fed SC or WD with HFCS for three months. Arrows indicate lipid-laden Kupffer cells which are marked with F4/80 (brown). Representative images were chosen from N=5 mice per group.

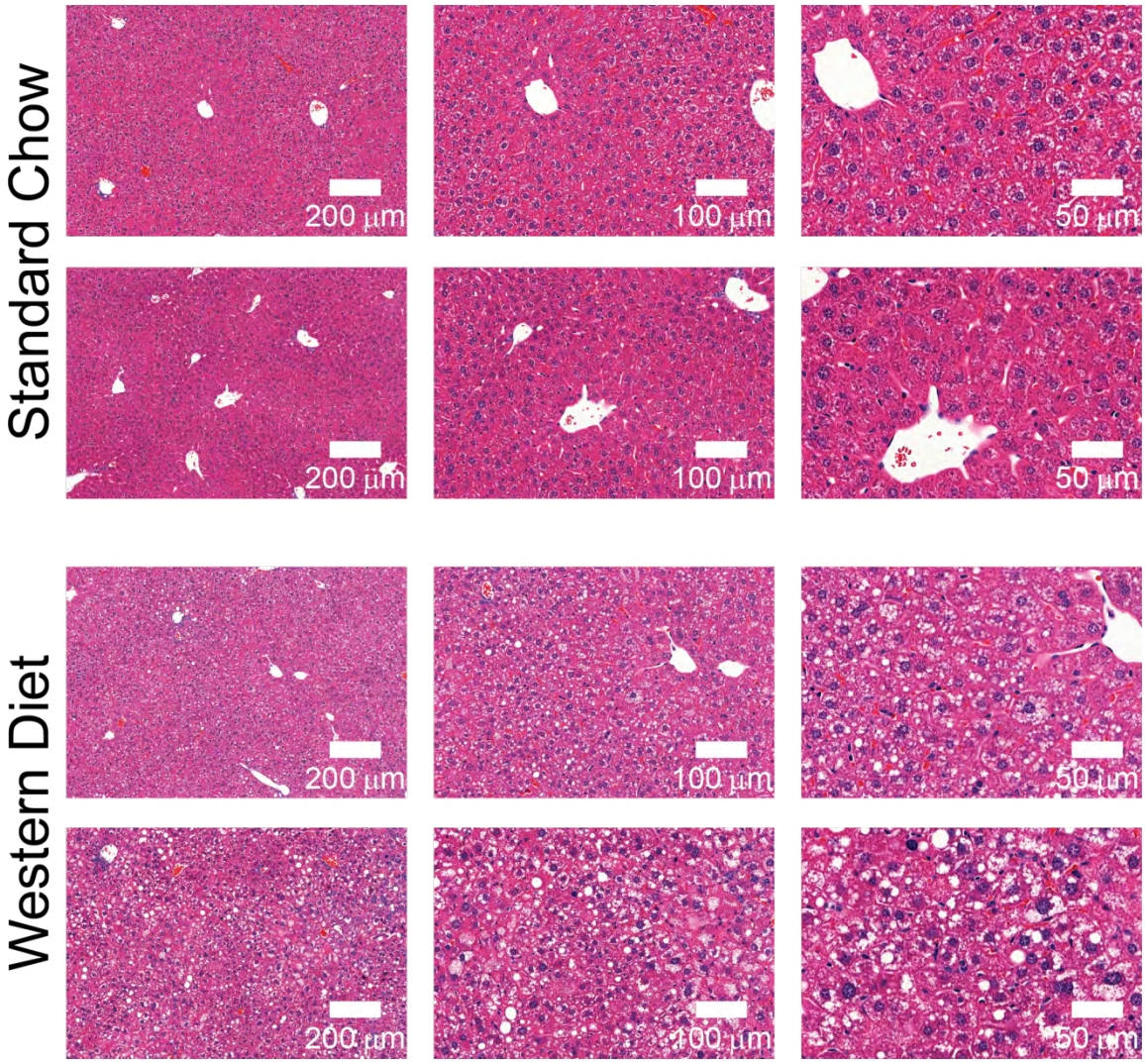

Fig. S26. Representative images of H&E stained liver tissues from C57BL/6 mice fed SC or WD with HFCS for one month. Representative images were chosen from N=3-4 mice per group.

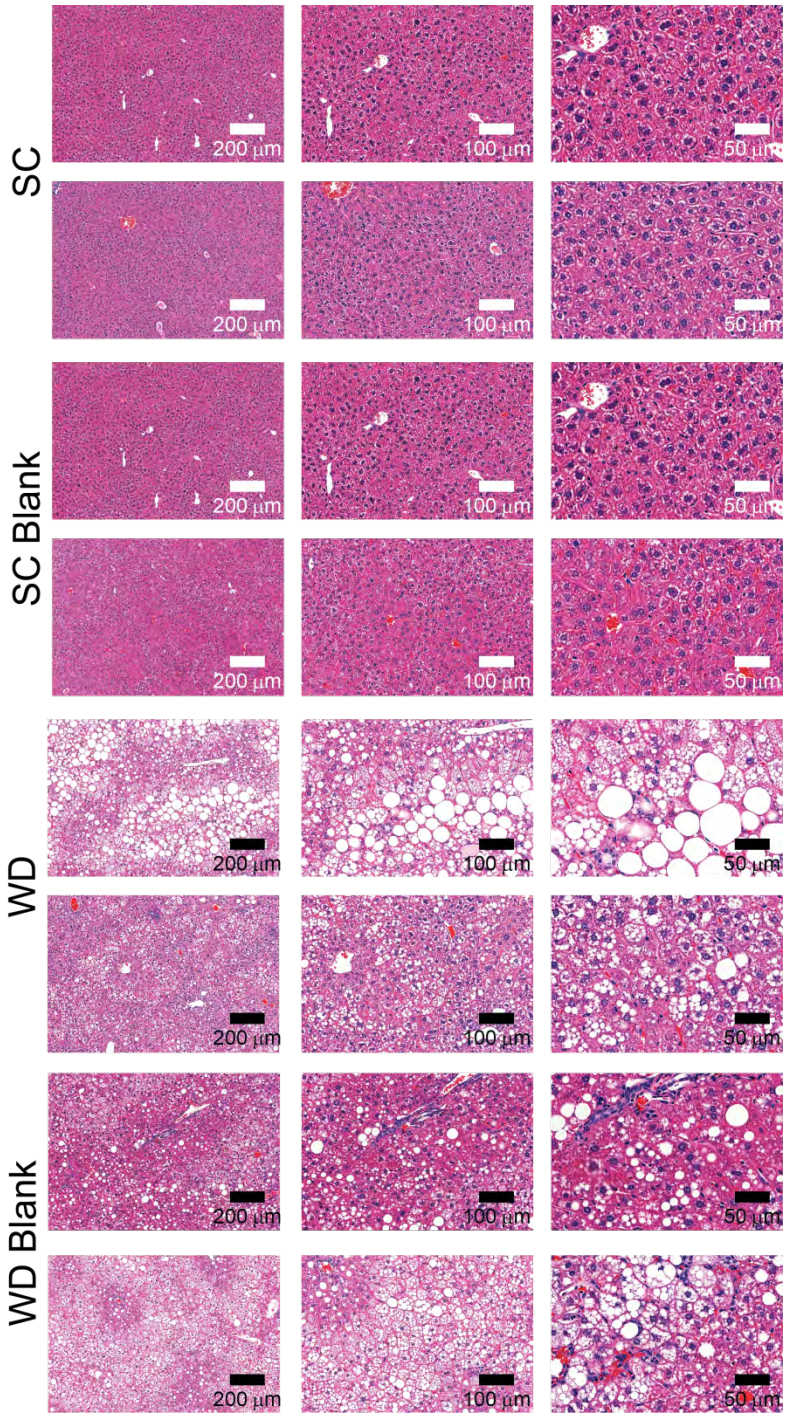

Fig. S27. Representative H&E stained liver tissues from mice fed SC or WD with HFCS for 3 months. "Blank" indicates these mice were not injected with the reporter, whereas other groups were injected intravenously with 200 ng of the reporter 24 hours prior to euthanization. Representative images were chosen from N=5 mice per group.

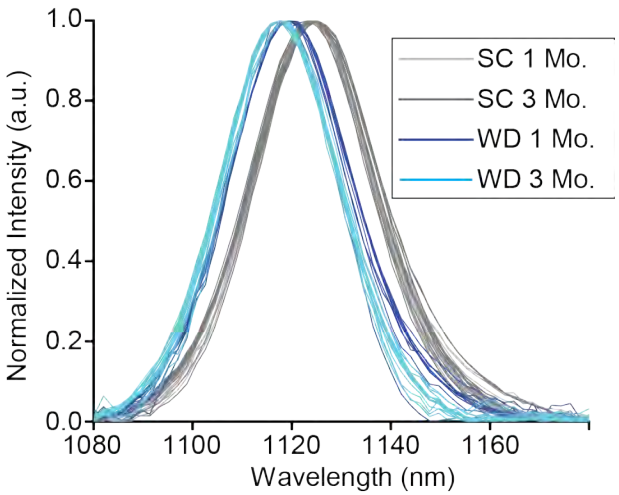

Fig. S28. In vivo emission spectra of the reporter from the liver of mice fed SC or WD with HFCS for 1 to 3 months. Emission spectra were measured 24 hours after intravenous injection of 200 ng of the reporter. Spectra shown represent multiple technical replicates taken from 3-5 different biological replicates per group.

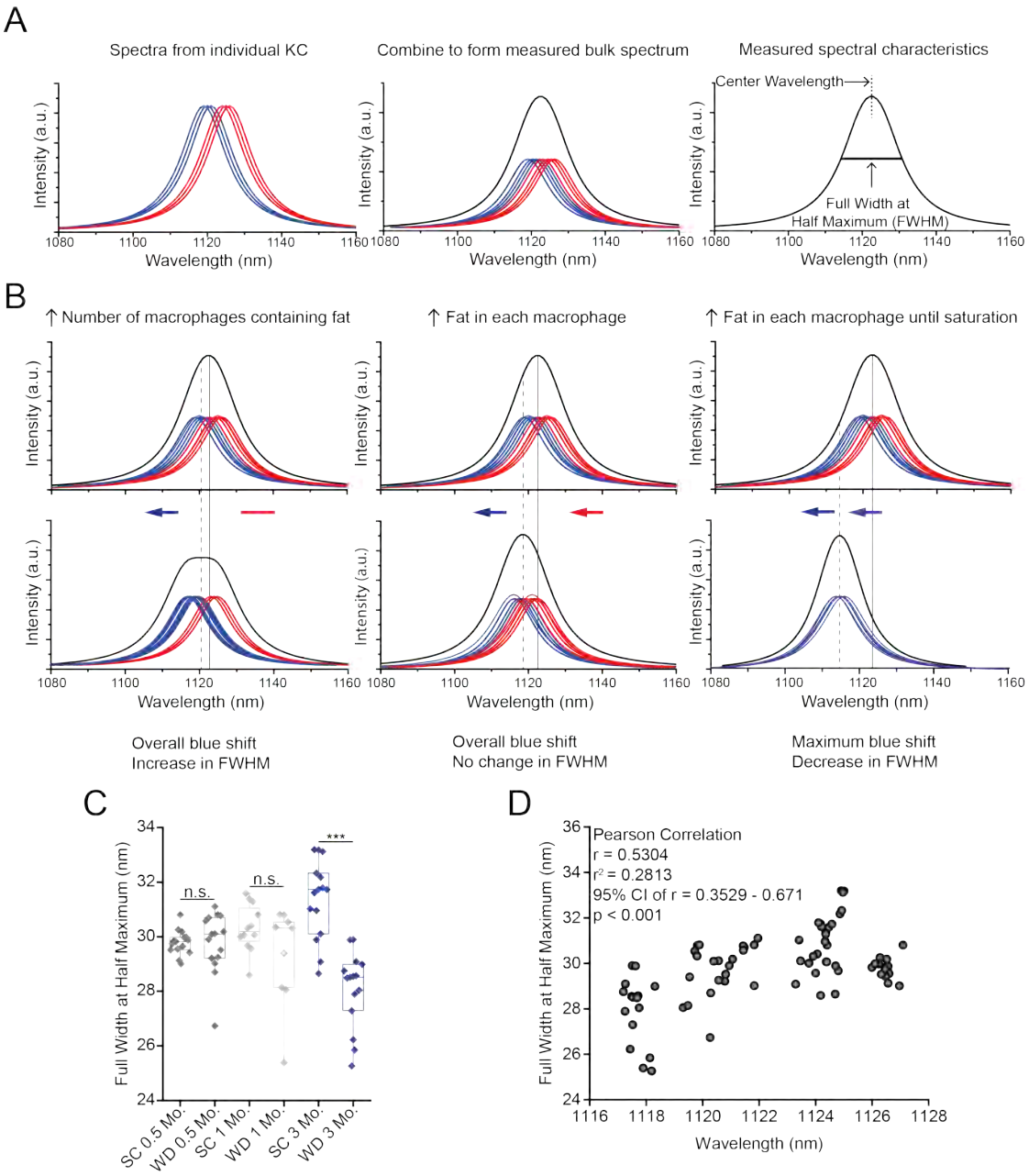

Fig. S29. Analysis of intercellular heterogeneity of Kupffer cell lipid content in vivo. (A) Schematic depicting the deconvoluted spectra of individual SWCNTs that combine to form the measured in vivo bulk spectra. **(B)** Schematic depicting expected results for three different scenarios pertaining to KC endolysosomal lipid accumulation. Red spectra in (A) and (B), represent KCs with lipid-poor endolysosomal organelles, while blue spectra represent KCs with lipid-rich endolysosomal organelles. **(C)** Spectral bandwidths denoted by full width at half

maximum (FWHM) of spectra taken in SC and WD mice. N = 9-15 per group. **(D)** Correlation analysis of FWHM vs. center wavelength. Pearson's correlation coefficient (r) = 0.5304 ($P < 0.001$), indicating a slight positive correlation between FWHM and reporter emission center wavelength.

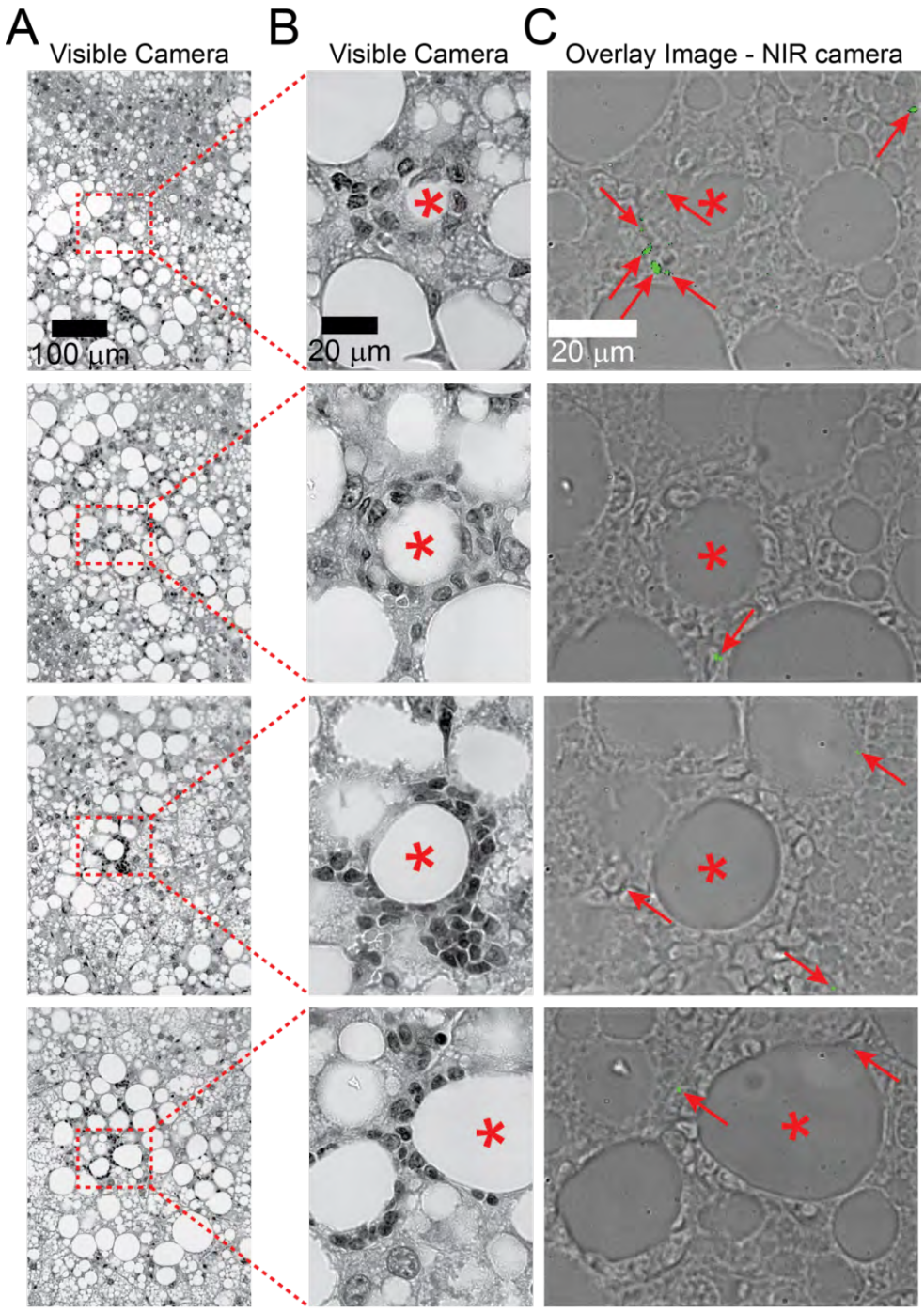

Fig. S30. Reporter presence in relation to lipogranulomas. (A) Transmitted light images of liver tissue taken on a traditional visible light camera. **(B)** Higher magnification images of tissues with lipogranulomas. **(C)** Overlay of near-infrared reporter emission (green, indicated with red

arrows) and transmitted light images acquired with a NIR camera. Fields of view are the same as in (B). Red asterisks indicate a common location in each image, as a reference.

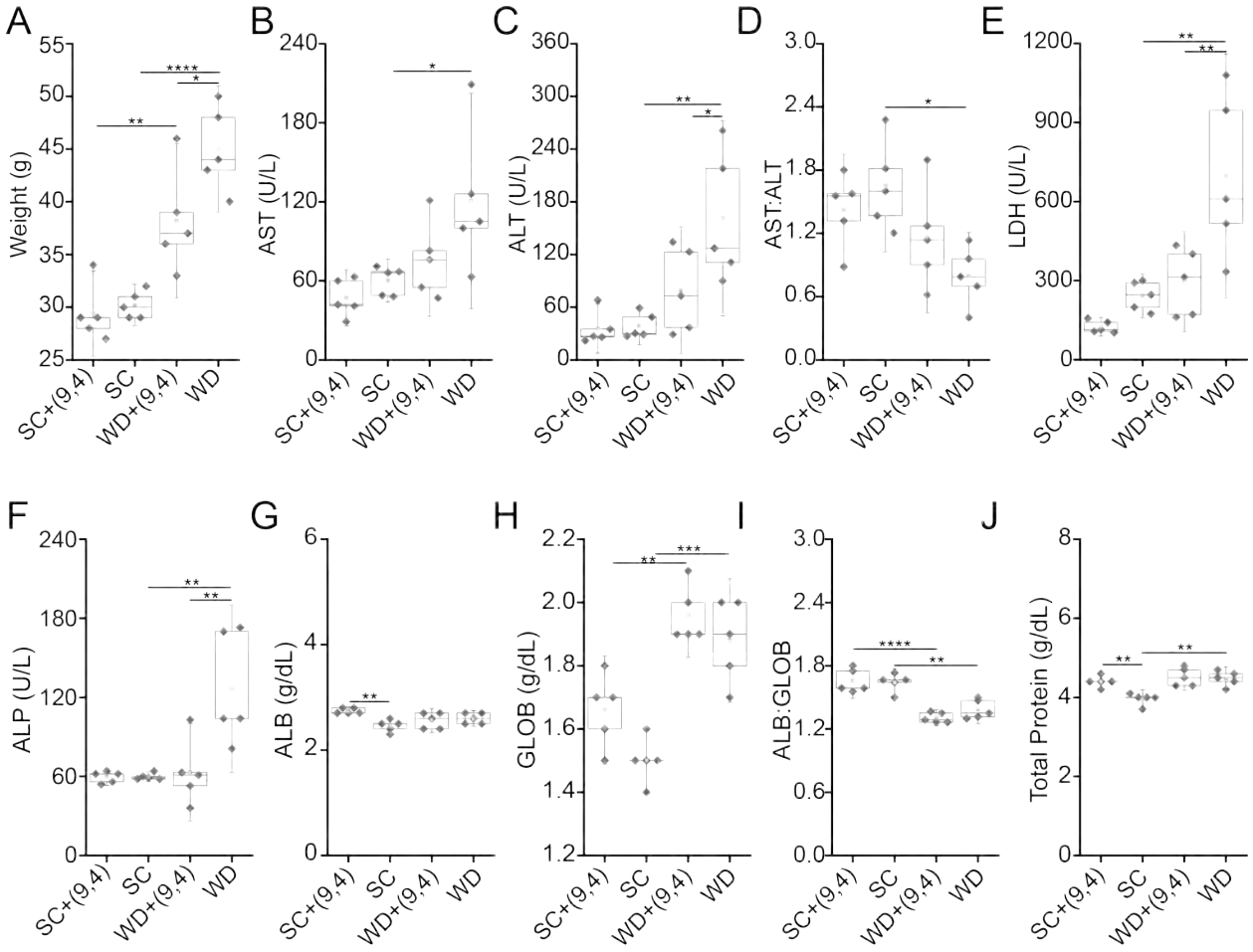

Fig. S31. Weight and serum chemistry measurements of mice fed SC or WD with HFCS for three months. "+ (9,4)" indicates mice that were injected with 200 ng of ssCTTC$_3$TTC-(9,4) whereas other groups were un-injected. All measurements were taken 24 hours after injection with ssCTTC$_3$TTC-(9,4). **(A)** Weight measurements of control and injected SC and WD mice after three months of feedings. **(B)** Serum aspartate transaminase (AST) concentrations in control and injected SC and WD mice. **(C)** Serum alanine transaminase concentrations (ALT) in control

and injected SC and WD mice. **(D)** Serum AST:ALT ratio in control and injected SC and WD mice. **(E)** Serum lactate dehydrogenase (LDH) concentrations in control and injected SC and WD mice. **(F)** Serum alkaline phosphatase (ALP) concentrations in control and injected SC and WD mice. **(G)** Serum albumin (ALB) concentrations in control and injected SC and WD mice. **(H)** Serum globulin (GLOB) concentrations in control and injected SC and WD mice. **(I)** Serum ALB:GLOB ratio in control and injected SC and WD mice. **(J)** Serum total protein concentrations in control and injected SC and WD mice.

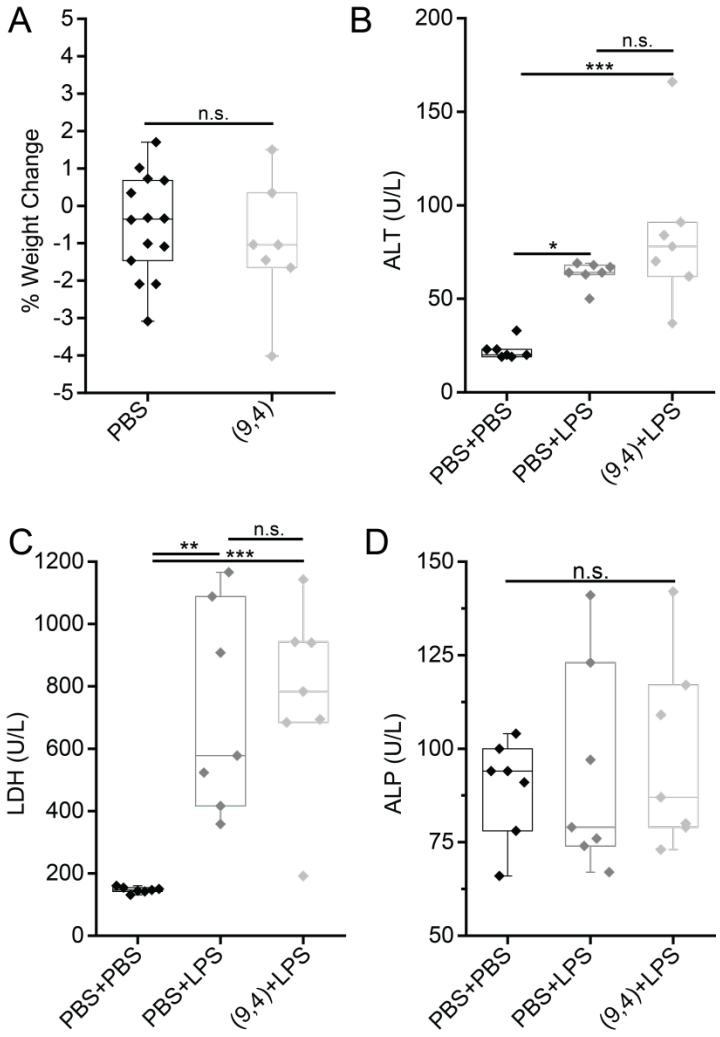

Fig. S32. Serum chemistry measurements and weights of reporter- and vehicle-injected mice in a model of hepatic injury. (A) Weight change in mice 24 hours after intravenous injection with the reporter or PBS. In experiments depicted in A-C, reporter or vehicle intravenous injections were performed 24 hours prior to LPS injections. **(B)** Serum alanine aminotransferase (ALT) concentrations in reporter or vehicle-injected (PBS) mice six hours after administration of lipopolysaccharide (LPS). **(C)** Serum lactate dehydrogenase (LDH) concentrations in reporter- or vehicle-injected mice six hours after administration of LPS. **(D)** Serum alkaline phosphatase (ALP) concentrations in reporter- or vehicle-injected mice six hours after administration of LPS. n.s. = not significant * = $P < 0.05$, ** = $P < 0.01$, *** = $P < 0.001$ as

measured with a one-way ANOVA with Tukey's post test or Student's t-test where appropriate. n=7 for A-C, n=7-14 for D.

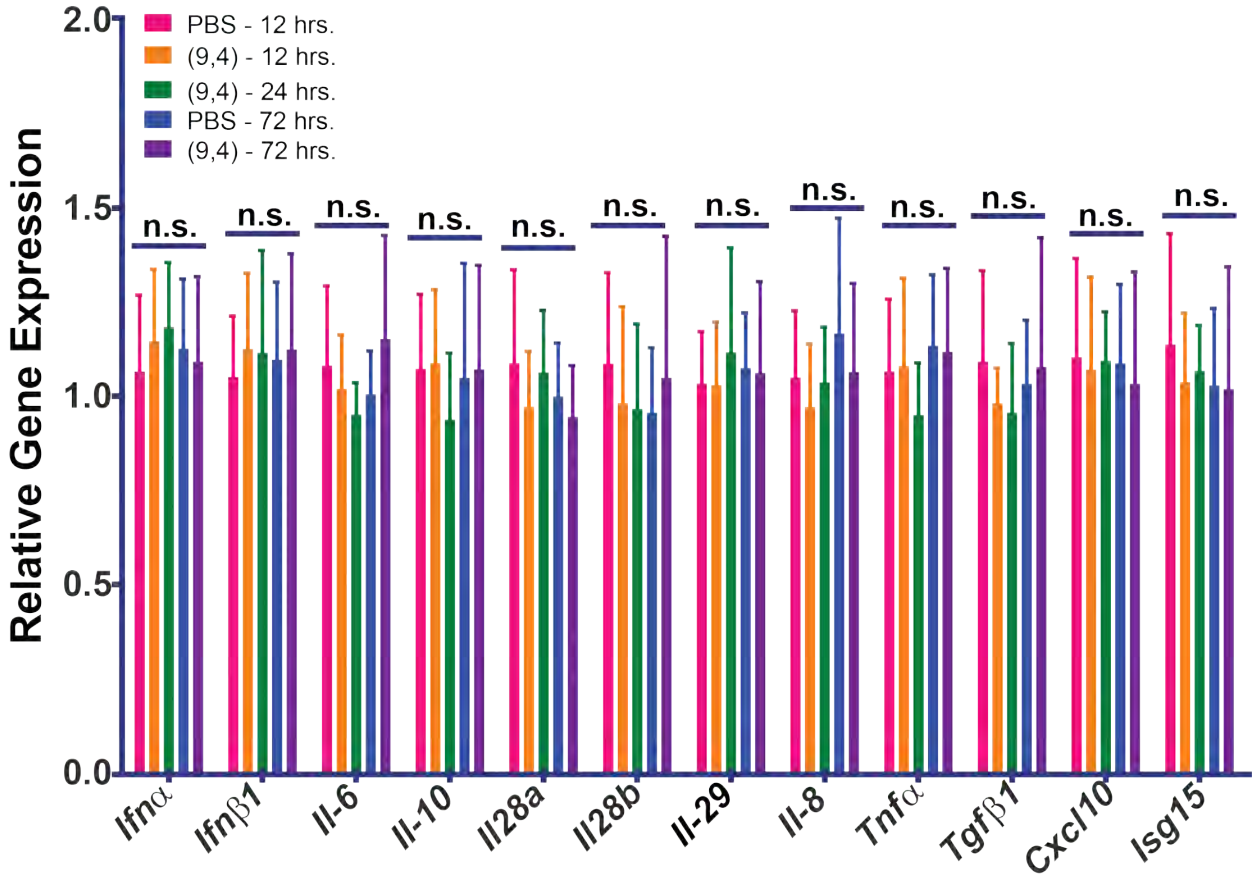

Figure S33. Relative expression of genes involved in the innate immune response after injection with ssCTTC3TTC-(9,4) or PBS. Statistical significance ($P < 0.05$) was determined with a one way ANOVA with Bonferroni's multiple comparison test. Error bars represent standard deviation, N=4 mice per group.

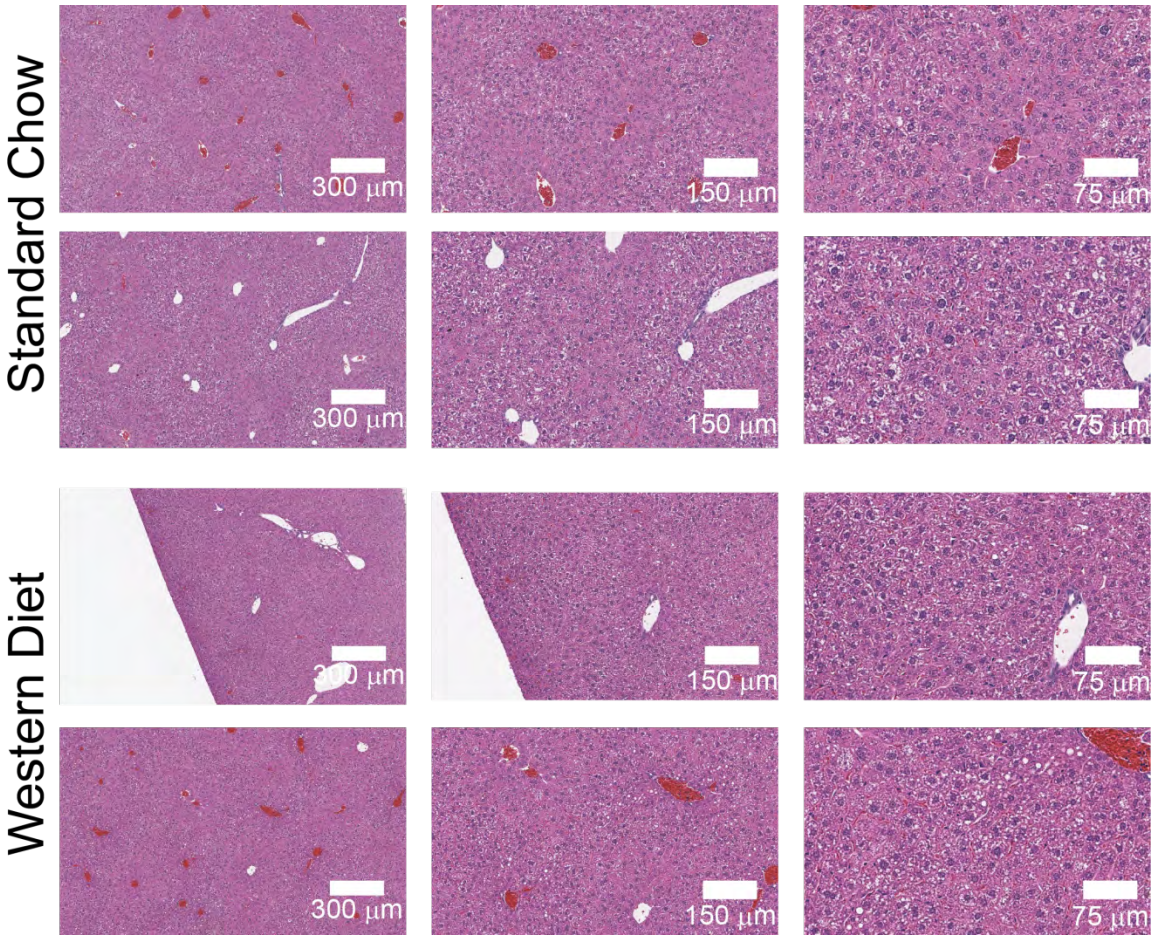

Fig. S34. Representative images of H&E stained liver tissue from C57BL/6 mice fed SC or WD with HFCS for two weeks. Representative images were chosen from N=5 mice per group.

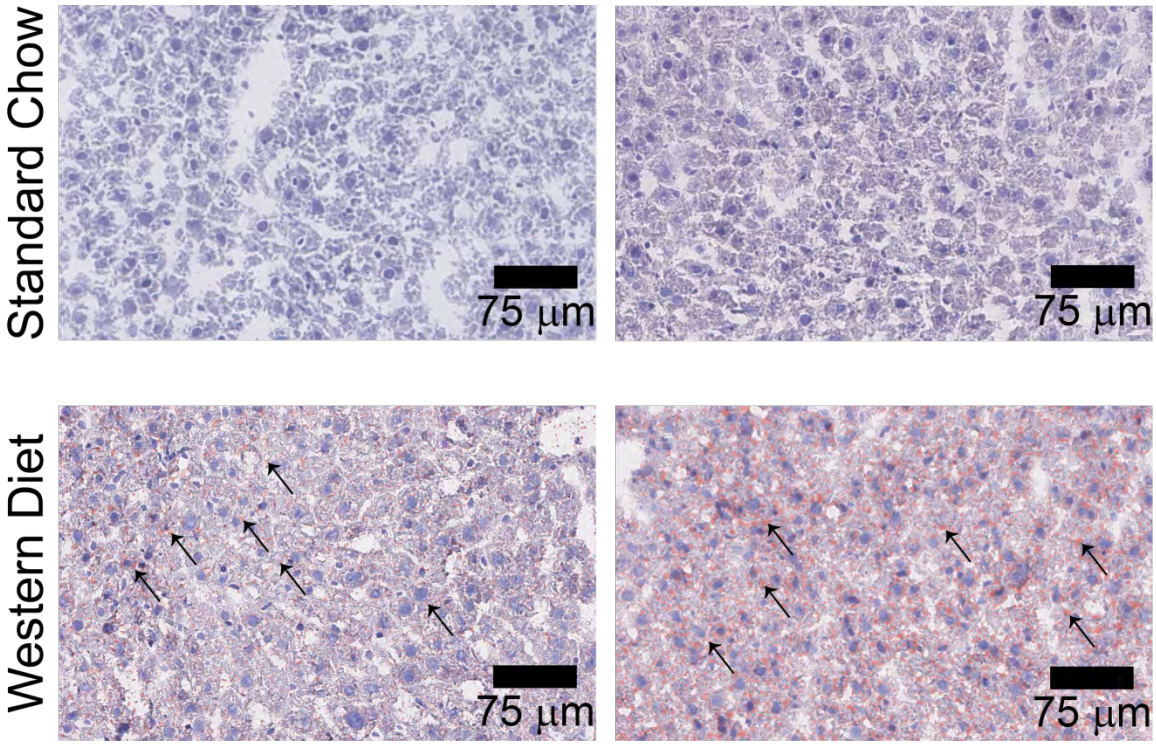

Fig. S35. Representative images of liver tissue stained with Oil Red O neutral lipid stain. Sections are from C57BL/6 mice fed either the WD with HFCS or SC for two weeks. Arrows indicate areas of positive Oil Red O staining. Representative images were chosen from N=5 mice per group.

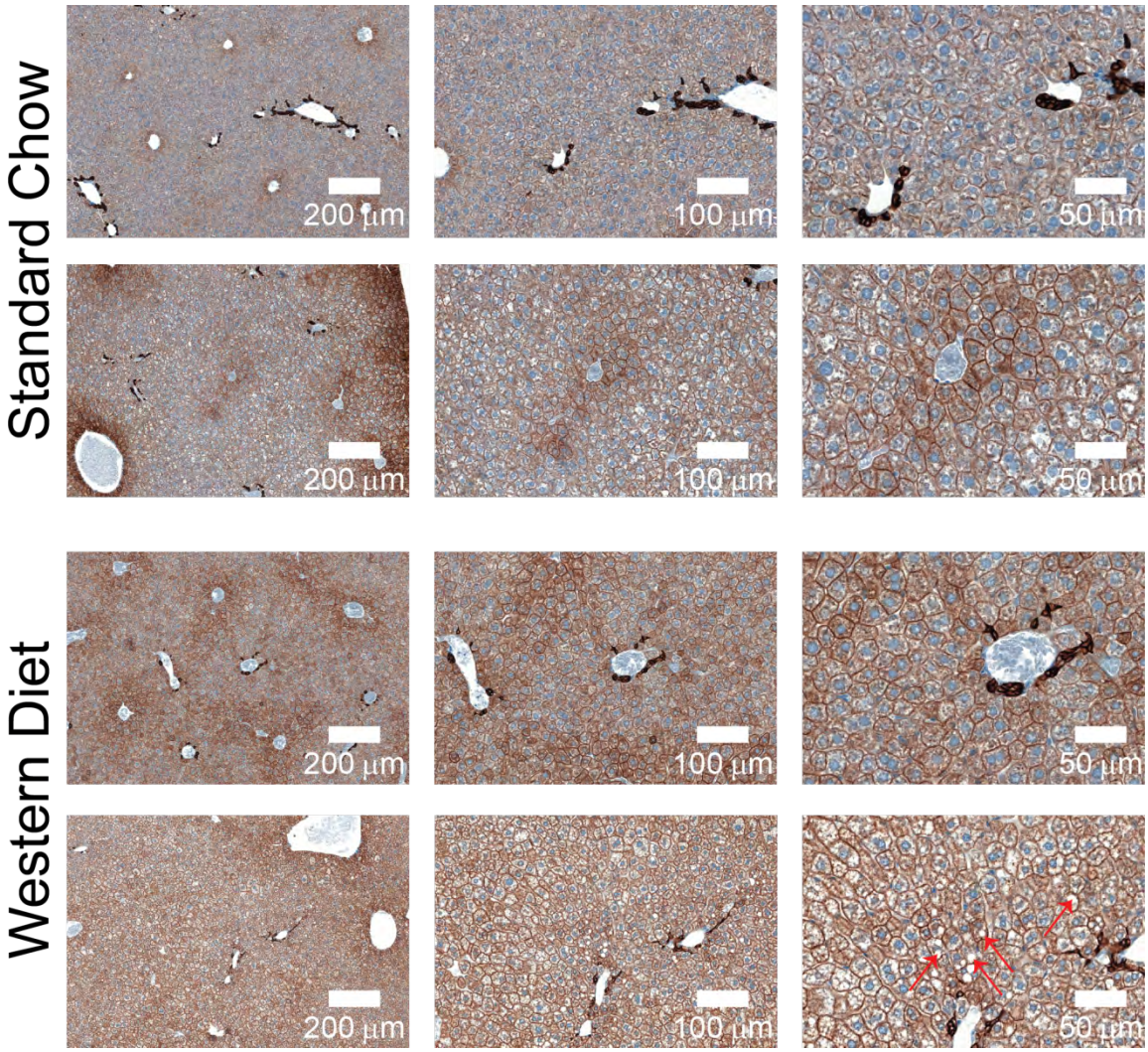

Fig. S36. Representative images of hepatic tissue from mice fed SC or the WD with HFCS for two weeks stained with the hepatocyte marker CK8/18. Arrows indicate lipid-laden hepatocytes (marked in brown). Representative images were chosen from N=5 mice per group.

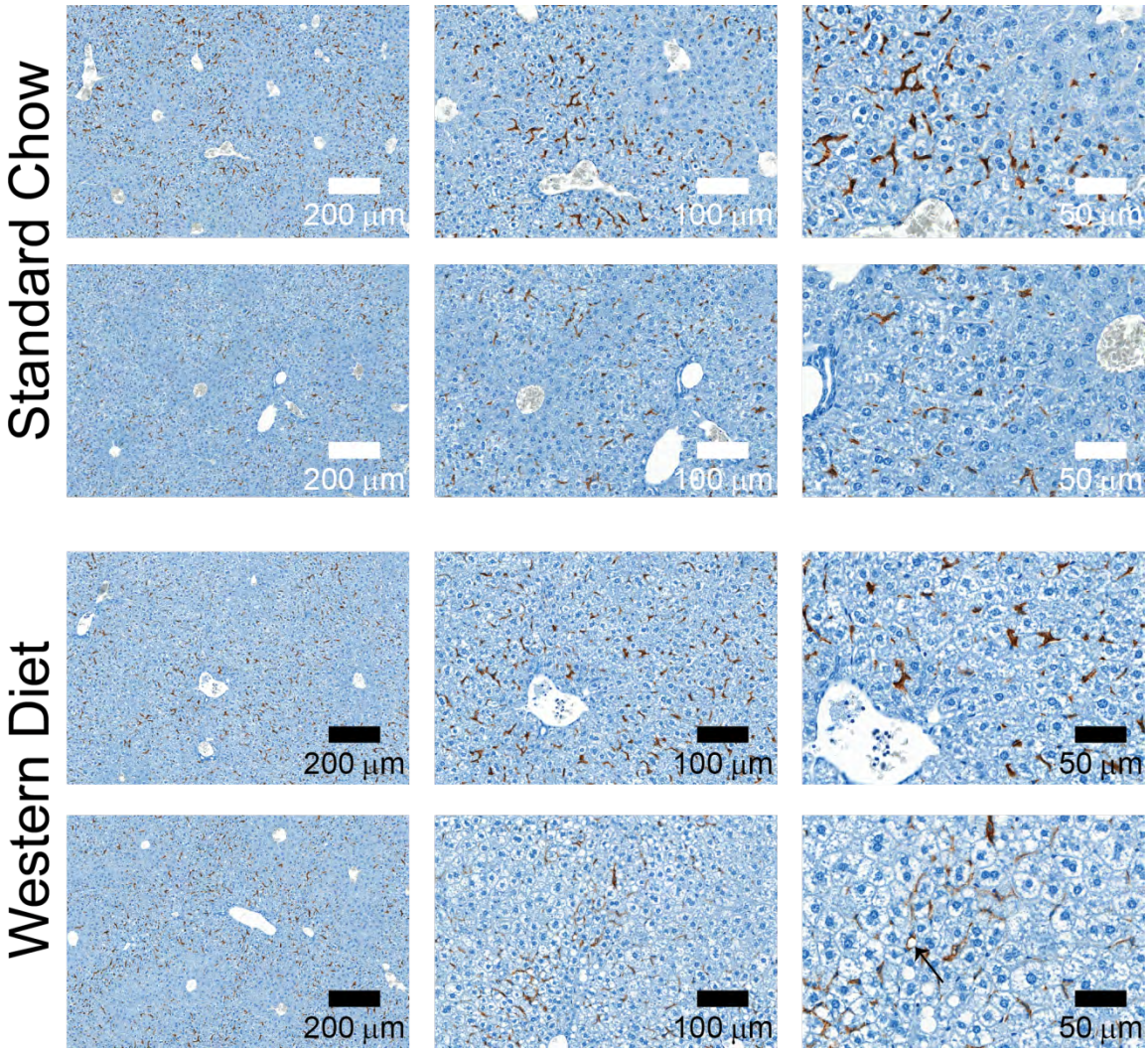

Fig. S37. Representative images of hepatic tissue from mice fed SC or the WD HFCS for two weeks stained with the Kupffer cell marker F4/80. Arrows indicate lipid-laden Kupffer cells (marked in brown). Representative images were chosen from N=5 mice per group.

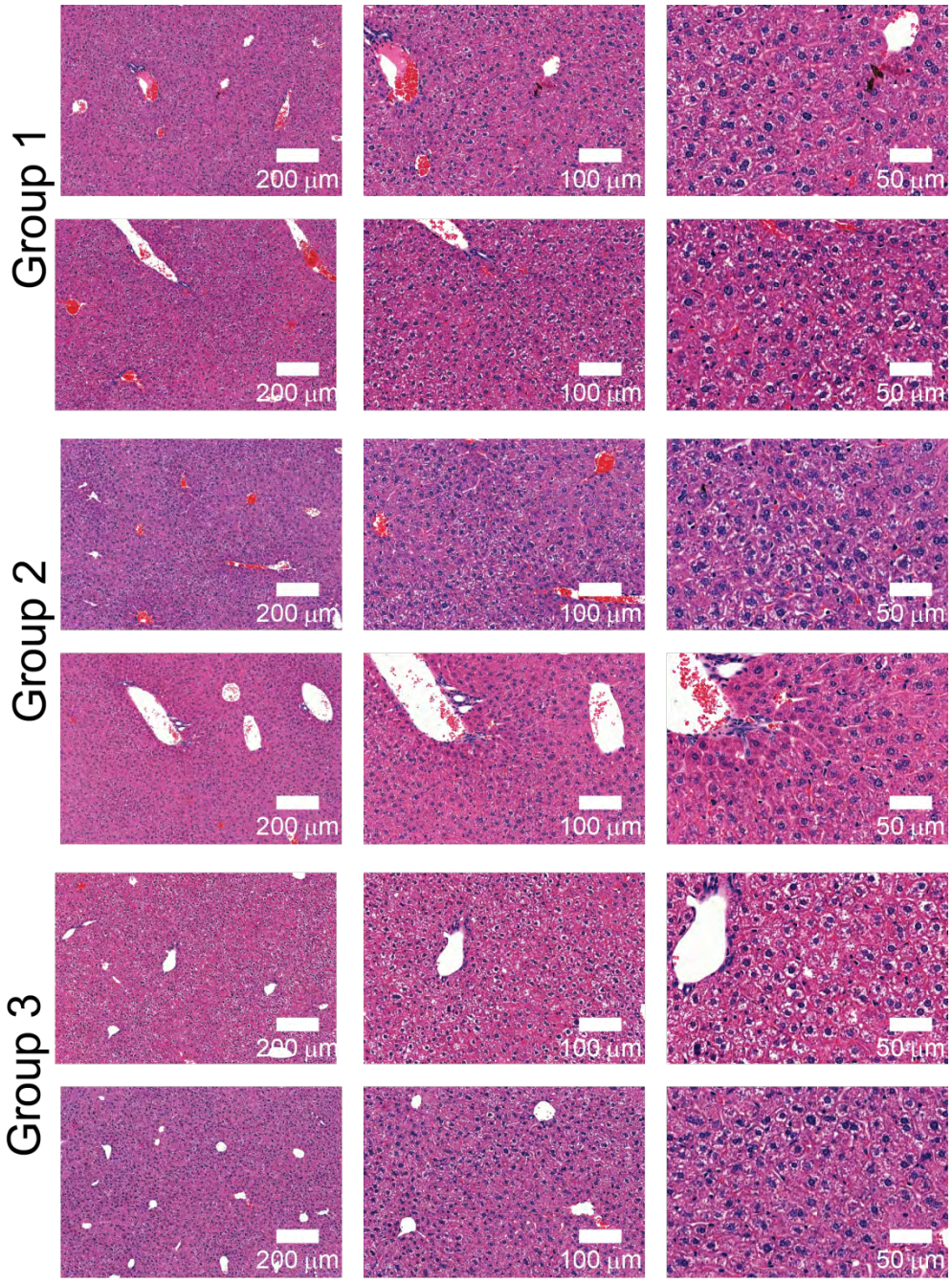

Fig. S38. Representative H&E sections of livers from mice shown in Fig. 5E. Representative images were chosen from N=5 mice per group.

Table S1. Average reporter emission center wavelengths measured from wild type and ASMKO mice in vivo, ex vivo, and in frozen sections of resected liver tissue.

Measurement	ASMKO Center Wavelength	Wild Type Center Wavelength
In vivo	1116.29 ± 0.16	1120.48 ± 0.21
Ex vivo	1117.48 ± 0.24	1120.72 ± 0.38
Resected Tissue	1118.94 ± 0.21	1121.53 ± 0.67

Table S2. Average reporter emission center wavelengths measured from wild type and $Npc^{tm(I1061T)Dso}$ mice in vivo, ex vivo, and in frozen sections of resected liver tissue.

Measurement	$Npc^{tm(I1061T)Dso}$ Center Wavelength	Wild Type Center Wavelength
In vivo	1119.22 ± 1.4	1124.47 ± 0.71
Ex vivo	1119.84 ± 0.1.67	1124.86 ± 0.82
Resected Tissue	1118.94 ± 0.21	1121.53 ± 0.67